Frequency Scanned Composite Right-Left Handed Leaky-Wave Antennas in Cognitive Radio enabled Long Term Evolution Advanced Home eNode-Bs

Rajib Chowdhury

A Thesis Submitted In Partial Fulfillment for the Degree of Master of Engineering

McGill University
April 2012

ABSTRACT

Long Term Evolution Advanced (LTE-A) is the further evolution to Long Term Evolution (LTE), a standard defined by the 3rd Generation Partnership Project (3GPP). LTE-A meets or surpasses the International Mobile Telecommunications Advanced (IMT-Advanced) requirements defined by the International Telecommunication Union (ITU). The capacity, standardized data-rates and low-cost deployments are concerns challenging the flexibility of LTE and beyond in LTE-A. For instance, providing high data rates over a large portion of the cell entails the usage of high bandwidth, which is limited and/or often wasted. Cognitive radio (CR) can contribute in addressing this mean through its capability to sense, learn, and autonomously adapt to its environment in order to optimize usage of spectrum (licensed and unlicensed). Also, it is known that a small distance between transmitter and receiver in a wireless system increases the capacity of this link and creates dual benefits of higher quality and more spatial reuse. Overlaying femotcells in legacy macro-cellular networks can thus be beneficial. In LTE-Advanced, femtocell access points are referred to as Home eNode-Bs (HeNBs). Such user installed devices communicate with the cellular network over a broadband backhaul such as Digital Subscriber Line (DSL) or a separate radio frequency (RF) backhaul channel. Logically in femtocell solutions, the need for compactness also turns out to be far greater for antennas. Hence triggers the idea of applying metamaterials, i.e., artificial, effectively homogeneous materials exhibiting unusual properties not readily available in nature. This thesis presents the design and analysis of a frequency scanned Composite Right-Left Handed (CRLH) Leaky-Wave Antenna (LWA) in a CR enabled HeNB. The antenna is designed with wire-bonded interdigital capacitors (WBIDC). This CRLH LWA is proposed to be used as a secondary antenna to support bandwidth-hungry applications of primary or secondary users within the femtocell, at its edge and in cooperation with its neighboring sites. Results exhibit that backfire to endfire radiation patterns between -60 and 60 degree angles are achievable at the azimuth plane between 2.2 and 3.25 GHz, respectively. Broadside radiation is achieved at 2.6 GHz, which accommodates a frequency-division duplexing (FDD) band 7 in LTE on the downlink (DL).

RÉSUMÉ

Long Term Evolution Advanced (LTE-A) est la poursuite de Long Term Evolution (LTE), un standard défini par 3rd Generation Partnership Project (3GPP). LTE-A atteint ou dépasse les requis définis par International Telecommunication Union (ITU) du International Mobile Telecommunications Advanced (IMT-Advanced). La capacité, les taux de données normalisées et les bas coûts de déploiements sont des préoccupations contestant la souplesse de LTE et au-delà dans LTE-A. Par exemple, en fournissant des débits élevés sur une grande partie de la cellule implique l'utilisation de la bande passante élevée. Cela est limitée et/ou souvent gaspillée. La Radio Cognitive (CR) peut donc contribuer par sa capacité de détecter, d'apprendre, et de manière autonome, s'adapter à son environnement afin d'optimiser l'utilisation du spectre (sans licence). En outre, il est connu que d'une faible distance entre l'émetteur et le récepteur dans un système sans fil augmente la capacité de ce lien et crée un double avantage de meilleure qualité et plus de réutilisation spatiale. L'approche femtocell peut donc être bénéfique. Sous LTE-Advanced, les points d'accès femtocell sont appelés Home eNode-Bs (HeNBs). Ces dispositifs peuvent communiquer avec le réseau cellulaire sur une liaison terrestre à large bande tels que Digital Subscriber Line (DSL) ou sous une fréquence radio (RF) canal backhaul. En conséquence, la nécessité de compacité se révèle d'être beaucoup plus importante pour ses antennes. Et voici ce qui déclenche l'idée de l'application de métamatériaux, matériaux artificiels effectivement homogène présentant des propriétés inhabituelles qui ne sont pas disponibles dans la nature. Cette thèse présente la conception et l'analyse d'une Composite Right-Left Handed (CRLH) Leaky-Wave Antenna (LWA) dans une CR permis dans la HeNB. L'antenne est aussi conçue avec du fil-collé condensateurs interdigitaux (WBIDC). Cette CRLH LWA est proposée pour être utilisée comme une antenne secondaire pour supporter des applications gourmandes en bande passante des utilisateurs primaire ou secondaire dans le femtocell, à son bord et en coopération avec ses sites voisins. Les résultats présentées démontrent que les diagrammes de rayonnement sont réalisables aux angles de -60 à 60 degrés au plan d'azimut entre respectivement, 2.2 et 3.25 GHz. Rayonnement broadside est réalisé à 2.6 GHz. Cela respecte la bande 7 du frequency division duplexing (FDD) de LTE sur la liaison descendante.

ACKNOWLEDGMENTS

Thanks to my advisor Prof. Milica Popovich for her guidance, motivating words, flexibility and constructive feedback during the course of this research. Thanks to M. Yves Lemieux for his guidance in professionalism, engineering principles and mentorship. Thanks to Prof. Christophe Caloz, Dr. Van-Hoang Nguyen and M. Jules Gauthier for their comments in metamaterials and antenna manufacturing. Thanks to Prof. Robert Paknys and Prof. Christopher Trueman for their guidance in engineering values and areas in electromagnetics. A special thanks to my parents, Rezaul and Nahid and my sister Rakhee.

Table of Contents

List of Figures

List of Tables

List of Acronyms

3G	Third Generation
3GPP	Third Generation Partnership Project
4G	Fourth Generation
BS	Base Station
BW	Bandwidth
CA	Carrier Aggregation
CAD	Computer Aided Design
CN	Core Network
CoMP	Coordinated Multi-Point
CR	Cognitive Radio
CRLH	Composite Right-Left Handed
dB	Decibel
DC	Direct Current
DRPD	Dynamic Radiation Pattern Diversity
DSA	Dynamic Spectrum Allocation
DSL	Digital Subscriber Line
DXF	Drawing Exchange Format
EM	Electromagnetic
e-NB	Evolved-Node B
EPC	Evolved Packet Core
e-UTRAN	Evolved-UMTS Terrestrial Radio Access Network
FDD	Frequency Division Duplexing
GW	Gateway
HeNB	Home e-Node B
HetNet	Heterogeneous Network
HPBW	Half-power Beamwidth
IDC	Interdigital Capacitor
IL	Insertion Loss
IMT	International Mobile Telecommunications
IPSec	Internet Protocol Security
ITU	International Telecommunication Union
LC	Resonant
LH	Left-Handed
LHCP	Left Hand Circular Polarization
LTE	Long Term Evolution
LTE-A	Long Term Evolution-Advanced
LW	Leaky-Wave
LWA	Leaky-Wave Antenna
Mhrs	Man-hours
MIMO	Multiple-Input-Multiple-Output
MTM	Metamaterial
MU-MIMO	Multi-User MIMO
NB	Node B
NRI	Negative Refractive Index

O&M	Operation and Maintenance
OFDM	Orthogonal Frequency Division Multiplexing
OTA	Over-the-Air
PLH	Purely Left-Handed
PRH	Purely Right-Handed
PTFE	Polytetrafluoroethylene
QoS	Quality of Service
RAN	Radio Access Network
RAS	Remote Azimuth Steering
RBS	Radio Base Station
Rx	Receive
RET	Remote Electrical Tilt
RF	Radio Frequency
RH	Right-Handed
RHCP	Right Hand Circular Polarization
RL	Return Loss
RNC	Radio Network Controller
RXI	Radio Cross Connect Interface
SDR	Software Defined Radio
SM	Spatial Multiplexing
S-parameters	Scattering Parameters
SRR	Split-Ring Resonator
SU-MIMO	Single-User MIMO
TDD	Time Division Duplexing
TL	Transmission Line
TEM	Transverse Electromagnetic
Tx	Transmit
UE	User Equipment
UMTS	Universal Mobile Telecommunication System
UTRAN	UMTS Terrestrial Radio Access Network
VSWR	Voltage Standing Wave Radio
WBIDC	Wire-bonded Interdigital Capacitor
WCDMA	Wideband Code Division Multiple Access
WiMAX	Worldwide Interoperability for Microwave Access
WLAN	Wireless Local Area Network

1 INTRODUCTION

1.1 Motivation

The continuing growth in the number of mobile communication users challenges wireless broadband access standards. This increased demand for wireless services implies a need for efficient cellular radio networks. This means more efficient and capable radio links and systems, but also more efficient network deployments and tuning. Emerging fourth generation (4G) wireless broadband access standards will require support of data rates not previously achievable in compact mobile devices. In response, advancements to 3GPP Long Term Evolution (LTE) strive to achieve 100 Mb/sec downlink and 50 Mb/sec uplink peak speeds in ideal conditions. In the evolution of LTE, LTE Advanced (LTE-A) projects the possibility for peak data rates up to 1 Gb/sec in the downlink and 500 Mb/sec in the uplink and the possibility to provide high data rates over a large portion of the cell. The efficient use of wideband channels at frequencies as low as 700 MHz, advanced modulation techniques, and above all Multiple-Input-Multiple-Output (MIMO) antenna technology, amongst others, are researched upon to refine these possible advancements [1]. The debate between WiMAX (Worldwide Interoperability for Microwave Access) and LTE as the emerging 3.9/4G access technology of choice is driven to an output where forecasts predict that by 2013, operators will spend over $8.6 billion on LTE base station (BS) infrastructure alone [2].

The increase of mobile communication users in turn increases the demand for radio spectrum access and the need for co-existence and inter-working of heterogeneous networks. Most of today's BS systems, however, are not capable of spectrum sensing and are designed to operate in a specific frequency band using a specific, pre-ordained, spectrum access system [3]. Investigations of spectrum utilization also regularly show that not all the spectrum is in use at any one time. A "cognitive" radio (CR), therefore, that can sense and understand its local radio spectrum environment and identify temporary vacant spectrum and local users, has the potential to provide enhanced

communications services for bandwidth hungry applications, increase spectrum efficiency and minimize the need for centralized spectrum management in the LTE-A paradigm [4].

In the 3G Wideband Code Division Multiple Access (WCDMA) standard's architecture, the Radio Access Network (RAN) (e.g. UTRAN – Universal Mobile Telecommunication System (UMTS) Terrestrial Radio Access Network) is composed of Radio Network Controllers (RNCs) and Radio Base Stations (RBS) or NodeBs (NBs). One of the major changes in LTE is that the RAN architecture is flattened so that the RNC functionality is distributed among BSs. The LTE architecture consequently contains only one logical node, the eNodeB (eNB) [5].

Indeed, RNC functionalities are also distributed in femtocell access points in LTE-Advanced. These nodes are referred to as Home eNBs (HeNBs). Femtocells use low-power, low-cost cellular BSs. They are typically deployed indoors to improve coverage and provide high data rates. There are a number of economic factors that argue strongly in favor of femtocells, including the capacity improvements that are enabled by allowing user equipments (UEs) to transmit with very low power to a femtocell. With nearly 50% of phone calls and 70% of data traffic taking place indoors, there is high interest in femtocells among network providers and equipment manufacturers [46-47]. Of course, careful planning is required when overlaying macrocells with femtocells. It is important to consider factors like the isolation of the femtocell to the macrocell in order to avoid destructive interference from both sites.

With MIMO transmission schemes in LTE (e.g. transmit diversity, receive diversity, spatial multiplexing), forecasted in LTE-Advanced (e.g. enhanced Multi-User (MU)-MIMO, Coordinated Multi-Point (CoMP) transmission, a baseline of 4 x 2, 4 x 4 and even 8-12 antennas at the eNB for MIMO capabilities) and the proposed idea to aggregate spectrum through CR principles, there will be significant requirements on antenna systems. Antennas must (i) actively contribute in optimization, interference management and capacity enhancement, (ii) be called upon to be flexible to spectrum

changes and serve multiple-standards and (iii) have proven beam scanning abilities. Items (ii) and (iii) are addressed in this thesis with frequency-scanned Composite Right-Left Handed (CRLH) leaky-wave antennas (LWAs). These antennas are proposed to serve as secondary antennas in CR enabled HeNBs. This enables further support to primary and secondary users when conventional femtocell BS antennas are unable to cover the vacant spectrum available at a particular position within the coverage area.

Elaborating further, it is assumed that primary integrated femtocell BS antennas will radiate covering the frequency band of operation for this BS similar to legacy macrocell BSs. As the BS is CR enabled, it will also have the ability to learn, sense vacancies in spectrum and autonomously adapt to its environment. So with knowledge of position and frequency supported by (say) secondary UEs, the CR enabled HeNB can turn on the secondary antenna for support. The secondary antenna as designed in this thesis covers an angular radiation based on frequency scanning. The angle of this CRLH LWA can then be steered by frequency tuning.

During this research, the thesis author was involved full-time in industry in Core and Access areas. LTE works on antenna features were conducted from an eNB point of view. His roles and responsibilities did not directly include the design of remote azimuth steering (RAS) antennas. This is why working half-time on this thesis, his motivation was to pursue research interests through the design of MTM antennas for LTE. It is important to note that all LTE *evolution* opinions are the author's, and are not in any way representing any other entity.

1.2 Reconfigurable Base Station and Metamaterial Antennas

A comprehensive study on BS antennas for 3G and LTE was delivered in [47]. In particular, the paper presented reconfigurability in terms of beamforming. Beamforming antennas include the possibility to change the boresight, or azimuth direction (panning) as well as the beamwidth of the antenna (fanning). This adds further dimension to the elevation beam steering (achievable via mechanical and/or remote electrical tilt (RET)).

The paper also studied how three dimensional remotely reconfigurable beam antennas (with tilting, panning and fanning) enabled clear optimization and load balancing gains for a 3G UMTS network. Thus, approaches to address beamwidth reconfigurability in conjunction with MTMs and antennas are described in the following paragraph.

In [37], CRLH transmission line (TL) principles were presented. It was described that TL metamaterials (MTMs) exhibit both "left-hand" LH and "right-hand" RH properties for wave propagation. Further, [8, 9] demonstrated that CRLH TL MTMs can be applied in radiated wave devices. With the effectiveness of MTMs, the dimension of the antenna cross-section can be very small compared to the operating wavelength. In conjunction, it can enhance the directivity of the beam produced by the radiator. In [8], the authors elaborated the fact that backfire-to-endfire, including broadside radiation pattern was achievable with CRLH LWAs, a feature limited in conventional LWAs (uniform and periodic). The angle of a CRLH LWA can be steered either by frequency tuning or by LC tuning at a fixed operation frequency. The tuning of LC parameters is achieved by integrating varactor diodes in each cell of the CRLH structure.

With frequency scanning, keeping the voltage distribution the same across the unit cell, maximum broadside directivity can be achieved. A thorough analysis of the latter is shown in [9]. A LWA with wire-bonded interdigital capacitor (WBIDC) was proposed in [54]. The WBIDC in the CRLH LWA was designed by placing short circuits at the end of alternate fingers of the interdigital capacitors (IDCs). Cascaded combinations of WBIDC in series and vias at the stub ends in series were used. A comparison was made between IDC and WBIDC to report the performance of WBIDC and its advantages in higher frequencies.

Alternatively, voltage-scanning increases the beamwidth with the superposition of all the radiations as different cells radiate toward different angles. A potential MIMO application to the voltage-scanning method was presented in [53]. The CRLH LWA design consisted of two independent DC bias networks to improve impedance matching and beam steering. It allowed for the excitation of an infinite number of antenna

configurations while maintaining good impedance matching and high isolation between the two ports of the array. This antenna was designed to operate in the 2.45 GHz for Wireless Local Area Network (WLAN) MIMO.

It was further described in [9] that CRLH LWA does not require any corporate feeding network. In addition, it allows an arbitrary number of antenna elements, which may be arbitrarily spaced, and the number of which may even be dynamically controlled for real-time beam shaping. This was extended to MIMO applications and analyzed in [10, 11] with the introduction of dynamic radiation pattern diversity (DRPD). Further design optimizations of CRLH LWAs can also be found in [55].

Industry research of [6] and [17] favored principles of MTMs and CR, mentioning that radio challenges in future communication systems can be overcome with the latter. It is worth referring to [52], the first industry published paper on MTM applications for LTE MIMO. The paper proposed a dual resonance MTM antenna which occupies a volume of $\lambda_o/10 \; x \; \lambda_o/41 \; x \; \lambda_o/387$, where $\lambda_o = v_o/f$ is the wavelength (in meters) at the frequency of the antenna current and $v_o = 3 \times 10^8$ meters per second (m/s) is the speed of light. The simulation and measurement results of a two element MTM antenna array with different spacing were presented, including quantified values of antennas far-field envelope correlation measurements. The MTM antennas not only had good radiation efficiency but also showed low isolation and low far-field envelop correlation numbers. The paper demonstrated the antenna's ability to support the high data throughput in LTE.

Alternatively, applications of MTMs for BS antennas were suggested in [43, 50, 51]. In particular, the authors in [43] presented numerical examples for an epsilon near zero (ENZ) MTM cylindrical shell characterized as a LWA. The antenna was excited on its azimuthally symmetric leaky mode for conical beam at the UMTS band (~ 1.9 GHz). In order to achieve pencil-beams, higher order leaky-mode excitations were required with an epsilon negative (ENG) and ENZ MTM shell. However, there were limitations in terms of practical realization in the design of small inclusions for exhibiting the shell's desired behavior. Plasma-tube technology was suggested to complement the solution.

The authors in [50] presented an ENZ MTM radome to enhance the gain and reduce the beamwidth of a dual-polarized patch antenna. The antenna was operable in the WiMAX 3.5 GHz band. However, this antenna was limited in terms of reconfigurability. It was more suitable for fixed-point communication.

The authors of [51] demonstrated the effectiveness of placing a dipole in front of a metamaterial slab. Around the resonant frequency of the effective permeability, the slab acted as an artificial magnetic conductor. When the effective permeability was close to zero, the system behaved as a spatial filter. It allowed, for a given polarization, the transmission of only a few angular components around the broadside. The former and latter cases were shown numerically. The cases exhibited interesting properties for the application in BSs and presented some degree of reconfigurability. However, the bulk size added by the magnetic slab in addition to the dipoles is undesirable.

1.3 Thesis Contribution

The ambition of the thesis is to design and analyze a frequency-scanned CRLH LWA using WBIDC with conventional stubs. The value-added scanning reconfigurability achieved from this antenna provides benefits if used in a CR enabled HeNB. The reasoning for enabling CR in forecasted HeNBs in LTE-A is also described in this thesis. The candidate antenna is proposed to serve as a secondary antenna to support further bandwidth requirements of primary and secondary users based on their positioning within and at the edge of the femtocell. The outcome of this study will justify that CRLH LWAs are an attractive alternative to conventional phased arrays. They have the advantage of requiring only one radiating element, utilizing a very simple and compact feeding mechanism and not necessitating any phase shifters. They are also capable of backfire-to-endfire, including broadside beam tuning. Comparisons between conventional IDCs and WBIDCs are also described in the analysis.

1.4 Thesis Organization

Chapter 2 compares the UMTS and LTE architectures, justifies principles enabling merging CR in LTE-A BSs and discusses HeNBs. It also visits antenna fundamentals, and surveys transmission schemes in LTE and LTE-A. Chapter 3 discusses fundamentals of metamaterials, CRLH TL theory, LWAs and CRLH LWAs. Chapter 4 presents the novel antenna solution, its design principles, analysis, simulation results with Ansoft Designer, experimental validation inputs and a summary of the design contributions. Conclusions and future directions are presented in Chapter 5.

2 Access Technology Briefing

This chapter introduces LTE and compares UTRAN and LTE architectures. LTE-Advanced topics are considered to justify the use of CR. HeNBs are described and related to the topics described for LTE-A. BS antenna fundamentals are reviewed. Since the proposed antenna is in essence beamwidth reconfigurable for an LTE-Advanced node, the device may be subject to multi-antenna transmission principles. Therefore, a high-level outtake is conducted on diversity, multi-antenna transmission schemes for LTE and projected for LTE-A and HeNBs.

2.1 Cognitive Radio enabled LTE-Advanced Base Stations

LTE is a term employed in Third Generation Partnership Project (3GPP) with the goal of determining the long term evolution of UMTS. UMTS was also a 3GPP project utilizing the Wideband Code Division Multiple Access (W-CDMA) technology for the RAN [14]. The solution/design presented in this thesis is projected to be deliverable for LTE-Advanced, the further evolution of LTE. The ambition of the evolution is to reach and surpass the requirements of IMT-Advanced, as defined by ITU-R – enhancing capability and performance compared to current cellular systems. The 3G network architecture (UMTS) is compared to LTE/LTE-A's architecture in order to define a baseline to build the eventual solution. Section 2.1.1 reviews this comparison while sections 2.1.2 and 2.1.3 elaborate on candidate LTE-A topics applying CR. Section 2.1.4 discusses HeNBs and unifies the topics discussed in 2.1.1-2.1.3 for this femotcell node.

It is to note that the protocols (signaling) for the user plane and control plane for the interfaces in RAN are beyond the scope of the thesis. Details of the core network are also omitted for the sake of simplicity. LTE is exclusive to the packet switched domain whereas UTRAN may comprise of circuit switched and packet switched domains.

2.1.1 UTRAN and LTE Architectures

The UTRAN architecture is depicted in Figure 2-1. Note that the aggregator Radio Cross Connect Interface (RXI), Operation and Maintenance (O&M) nodes and the mobile backhaul for transport are omitted for simplicity. Figure 2-1's RAN consists of the Radio Base Stations (RBS, in 3GPP called Node B) and the Radio Network Controllers (RNC). The RBS is the interface towards the user equipment (mobile station) and provides the radio resources. The RNC manages Radio Access Bearers for user data, the radio network resources and mobility. It is the controlling node in the network [15]. The key external interfaces are the Iu interface between the RNC and the core network (both packet and circuit switched domains) and the Uu interface between the UE and the RBS. Within the RAN, the RNCs communicate with each other over Iur and with RBSs over Iub.

The LTE architecture is provided in Figure 2-2. The connection between the eNB and the Core network (i.e. Evolved Packet Core (EPC)) is made through the S1 interface. The function of S1 can be compared to Iub interface in a WCDMA system. The eNBs are connected to each other through the logical X2 interface. Its main function is the support of packet forwarding during UE mobility. The function of X2 can be compared to Iur interface in a WCDMA system.

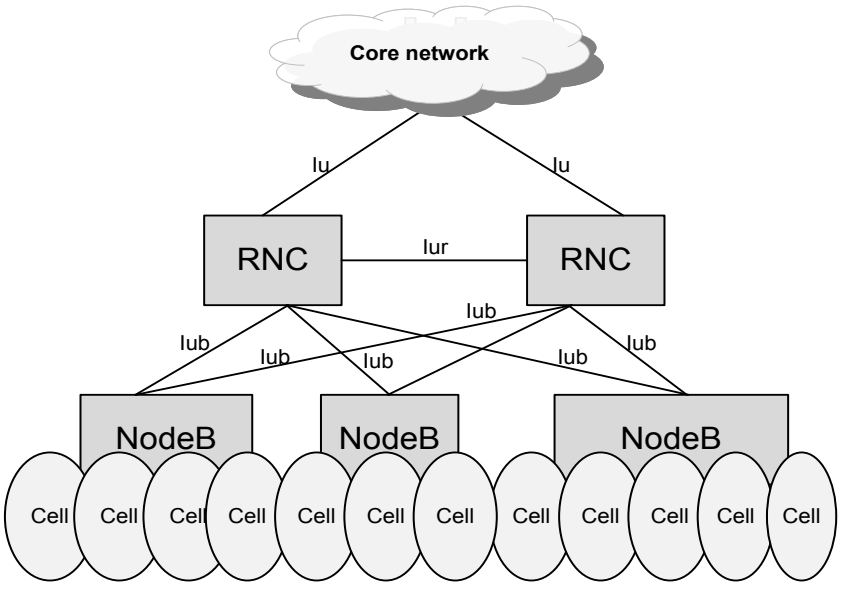

Figure 2-1: Simplified UTRAN architecture

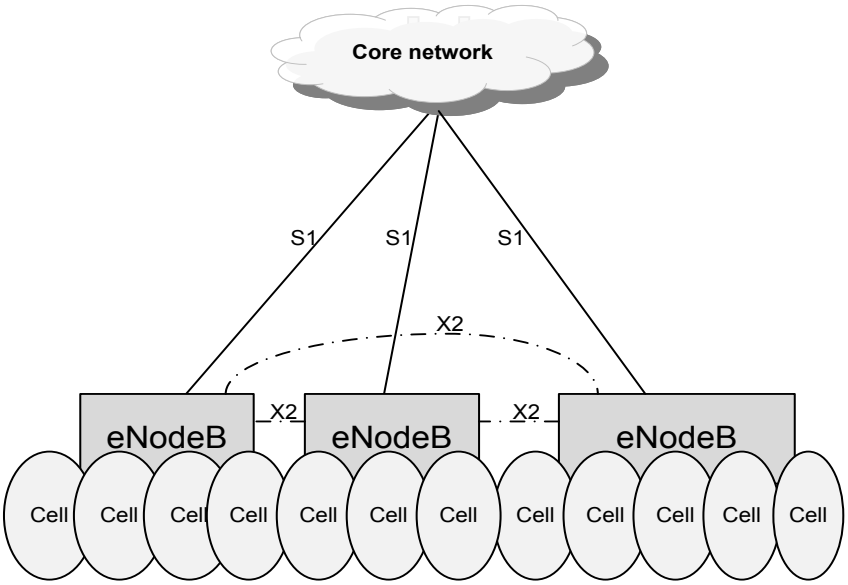

Figure 2-2: LTE architecture

This comparison shows that the LTE architecture is much simplified; an eNB now holds some of the functionalities of the RNC and RBS. This is the flattening idea presented in the introductory chapter. LTE-A also projects to hold a similar architecture for its nodes.

2.1.2 Increased Transmission Bandwidth in LTE-A

With LTE-A, bit rates are expected to reach 1 Gbit/s user data for nomadic users, and 100 Mbit/s for mobile users at downlink. To achieve such throughput, LTE-Advanced systems demand the usage of 100 MHz bandwidth. This amount of requested contiguous spectrum might be impossible to find.

It is observed however that the channels allocated for cellular systems are not always active in the frequency bands. Therefore, it is possible to increase bandwidth by aggregating these vacant channels [16]. This system is tentatively called a carrier aggregation (CA) system. In other words, separated frequency slots are combined to give the necessary effective bandwidth [17]. Two types of CA techniques have been proposed for the LTE-Advanced mobile systems: Continuous CA when multiple available component carriers are adjacent to each other and Non-continuous CA when multiple available component carriers are separated along the frequency band. In both cases

multiple LTE/component carriers are aggregated to serve a single unit of LTE-Advanced UE [16].

This feature fits well for the usage of CR, introduced by Mitola in [45]. CR projects the possibility to use parts of spectrum which are free in time and geographical location, in a very dynamic way. In fact, CR extends the notion of spectrum utilization distinguishing licensed (primary) and unlicensed (secondary) users. If the licensee is not using a band in a certain area, other "secondary" users could opportunistically use the spectrum. This spectrum management approach, called Dynamic Spectrum Access (DSA), could open up vast amounts of spectrum [19]. This can be utilized in scenarios where an operator accesses both a dedicated band and a spectrum sharing band, which is separated in frequencies from the dedicated operator's band.

2.1.3 Multi-Standard Radio Base Stations for LTE-A

BSs continue to get smaller yet offer higher performance. One of the most significant advances in BS technology is a flexible platform that supports multiple radio access technologies in a single RAN concept. This is achieved through the use of software-defined radio (SDR) and ultimately CR running on multi-standard baseband and RF hardware [20]. Different BS configurations means that several RBS nodes of same and different radio standards will be placed in the same cabinet, sharing climate, power etc. These RBS nodes have to also further cooperate to handle common radio units and RF equipments.

The ability to support the concepts defined in sections 2.1.2 and in this section calls for cognition and reconfigurability. Cognition is the ability of spectrum sensing across multi-bands, multi-standards and multi-channels to detect and classify RF activities of interest. It is also the ability to decide in which band under what standard the radio needs to establish communication with a chosen RF device. This device in a successful implementation should have built-in intelligence and cognition to effectively learn from its observations and past actions, and correct its behavior as necessary in realtime [21]. Reconfigurability is the ability to adapt RF communications parameters, such as standard,

carrier frequency, transmit power, modulation format, coding scheme and its rate, without having to change hardware [22].

2.1.4 Home eNB

Home eNB (HeNB) is developed as a small low-cost BS installed by the subscriber with a short service range (i.e., 10 to 30m). Such user-installed femtocell BSs communicate with the cellular network over a broadband backhaul such as DSL. The functionality of HeNBs is almost the same as that of the typical macro eNB discussed in 2.1.1. Concurrently, the price of a HeNB can be significantly lower because it serves a small number of users and a relatively low transmit power is enough to cover the service area.

The simplified architecture of the HeNB is presented in Figure 2-3. For further simplicity, the description is limited to the E-UTRAN femtocell nodes.

An Internet Protocol Security (IPSec) tunnel is created between the HeNB to a Security Gateway (GW) in the operator network. Security can also be managed by extra SIM in HeNB. The (optional) HeNB GW provides the access of the HeNB to the operator's Core Network (CN) or Evolved Packet Core. This GW is responsible for protocol conversion and also creates a virtual radio network control interface to the EPC without requiring changes to the CN elements. It is located at the operator's premises.

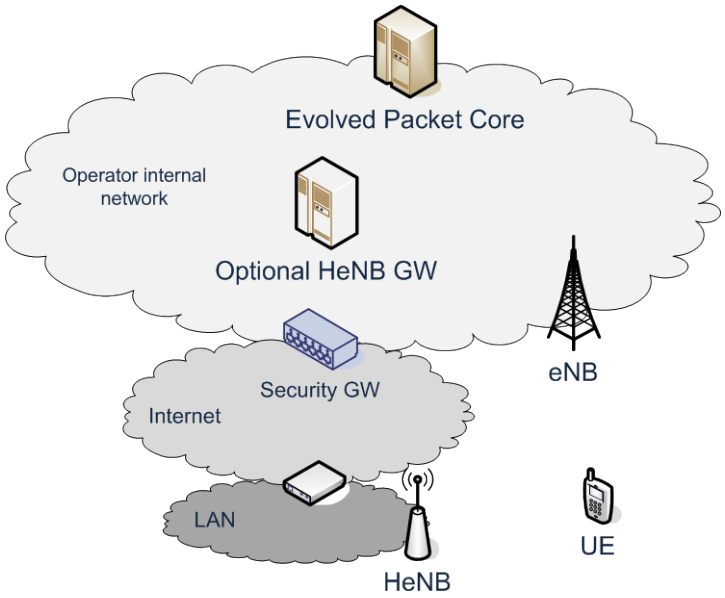

Figure 2-3: Simplified femtocell network

One network deployment scenario where flexible spectrum use is beneficial is the Heterogeneous Network (HetNet) deployment, where macro (public) cells share the spectrum with many femtocells (and/or HeNBs). Figure 2-4 depicts this idea, showing macrocell networks and TV broadcast systems coexisting with femtocells. This type of overlay in access networks further inspires concepts of CR as initiated in section 2.1.2. In this case, CR-enabled femtocell users and HeNBs can identify and utilize the spectrum opportunities from the licensed microcell and TV broadcast systems [7]. Further, if the HeNB evolves as a multi-standard BS, cognition and reconfigurability concepts as described in section 2.1.3 can also come into effect. It is considering these concepts and the transmission schemes described in section 2.2 that the antenna solution proposal is built in chapter 4.

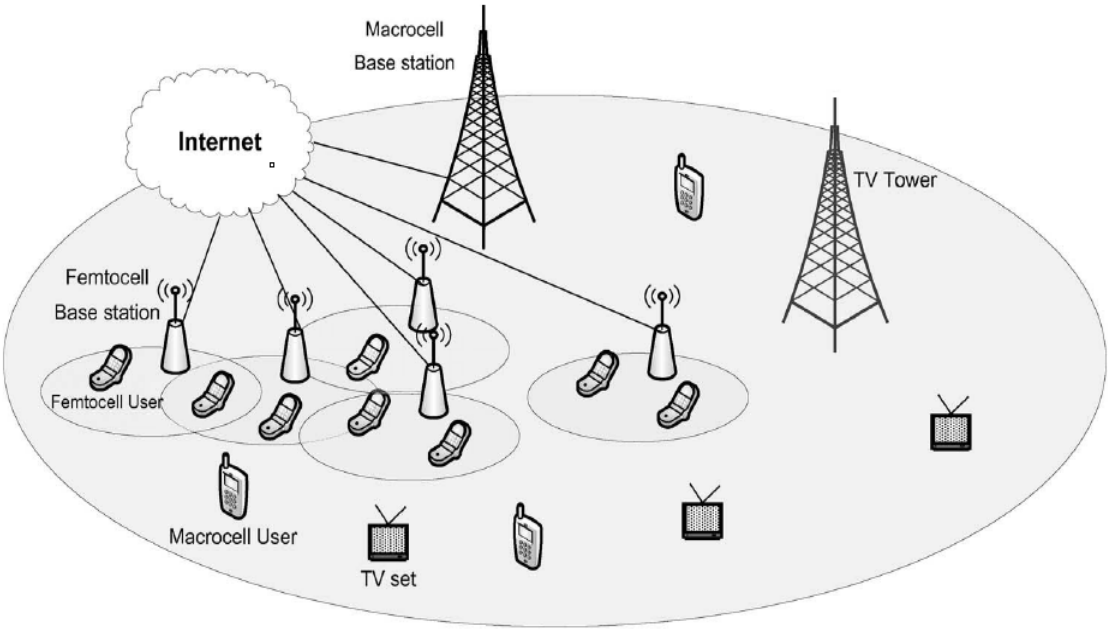

Figure 2-4: Coexisting CR femtocells and primary systems such as macrocells and TV systems. Adapted from [7]

2.2 Antennas and Transmission Schemes

This section starts with a briefing on antenna fundamentals and progresses on smart antennas. The concept of diversity is described. MIMO transmission schemes applicable in LTE are overviewed. In particular, receive diversity, transmit diversity and spatial multiplexing are visited. For LTE-Advanced, coordinated multi-point transmission (CoMP) is introduced.

2.2.1 Antenna Parameters

2.2.1.1 Near-Field and Far-Field Regions

Close to the antenna, the field patterns change rapidly with distance and include both radiating energy and reactive energy, which oscillates towards and away from the antenna and appears as a reactance. This reactance only stores, but does not dissipate energy. Further away, the radiating energy is present but the reactive fields are negligible. This results in a variation of power with direction independent of distance [26].

Conventionally, these regions transit at a radius R given by

$$R = \frac{2D^2}{\lambda} \tag{2-1}$$

where D is the largest dimension of the antenna and λ is the wavelength. Within the radius is the near-field or Fresnel region. Beyond the radius is the far-field or Fraunhofer region. The far-field region is the region where the angular field of an antenna is independent of the distance from the antenna.

2.2.1.2 Fields and Power Radiation

The far-field electromagnetic fields radiated by an antenna are described in this section. The considered antenna is located at the origin of the spherical coordinate system in Figure 2-5 [60]. At large distances, where near-field patterns are negligible, the expression of the radiated electric field of an arbitrary antenna is

$$\overline{E}(r,\theta,\phi) = [\hat{\theta}F_{\theta}(\theta,\phi) + \hat{\phi}F_{\phi}(\theta,\phi)]\frac{e^{-jk_o r}}{r} \tag{2-2}$$

where $\overline{E}$ is the electric field vector in volts per meter (V/m), $\hat{\theta}$ and $\hat{\phi}$ are unit vectors in the spherical coordinate systems, r is the radial distance from the origin in meters (m), $k_o = 2\pi/\lambda_o$ is the free-space propagation constant and $F_\theta(\theta,\phi)$ and $F_\phi(\theta,\phi)$ are the pattern functions. $\overline{E}$ propagates in the radial direction, with a phase variation of $e^{-jk_o r}$ and an amplitude variation of $1/r$. The polarization of $\overline{E}$ is either in the $\hat{\theta}$ or $\hat{\phi}$ directions but not the radial direction. These are some characteristics of transverse electromagnetic (TEM) waves [60]. When there is a propagating electric field, there is an associated magnetic field. For the TEM wave of (2-2), the magnetic fields are expressed as

$$H_\phi = \frac{E_\theta}{\eta_o} \tag{2-3}$$

$$H_\theta = \frac{-E_\phi}{\eta_o}, \tag{2-4}$$

where η_o = 377 Ohms (Ω), the wave impedance in free space. The magnetic vector is polarized only in the transverse direction [60]. The Poynting vector for electromagnetic fields, in watts per meter squared (W/m^2), is given by the cross product of electric and magnetic field vectors:

$$\overline{S} = \overline{E} \times \overline{H}^* \tag{2-5}$$

and the time average Poynting vector is

$$\overline{S}_{avg} = \frac{1}{2}\mathrm{Re}\{\overline{S}\} = \frac{1}{2}\mathrm{Re}\{\overline{E} \times \overline{H}^*\}. \tag{2-6}$$

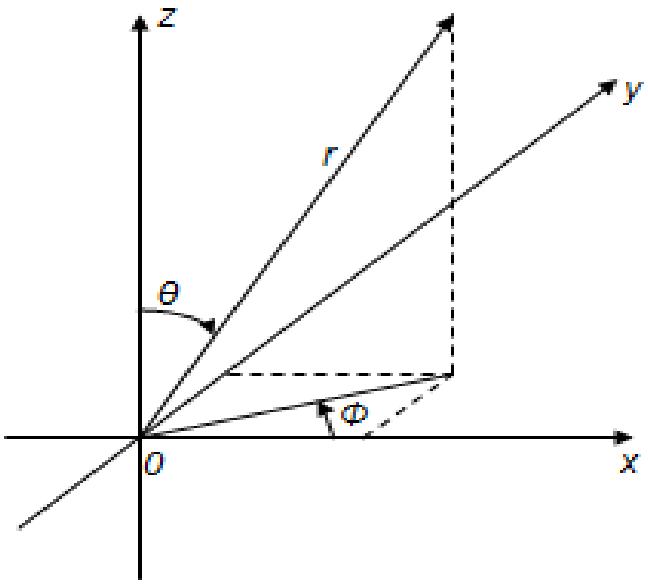

Figure 2-5: Spherical coordinate system

2.2.1.3 Radiation Pattern

The radiation pattern describes how an antenna focuses or directs the energy it radiates or receives. The antenna does not act as an absolute power amplifier, rather, it acts as a directional amplifier, transmitting or receiving energy in one specific region of space more so than others. The radiation pattern of an antenna is a plot of the relative power versus angle. It can be plotted from the pattern functions $F_\theta(\theta,\phi)$ and $F_\phi(\theta,\phi)$, versus either the angle θ (for an elevation plane pattern) or ϕ (for an azimuth plane pattern) [60]. A radiation pattern plot of a generic directional antenna is illustrated in Figure 2-6. This schematic illustrates the main lobe, which includes the direction of the maximum radiation i.e., boresight direction, a back lobe of radiation diametrically opposite to the main lobe, and side lobes which are the lobes at lower levels.

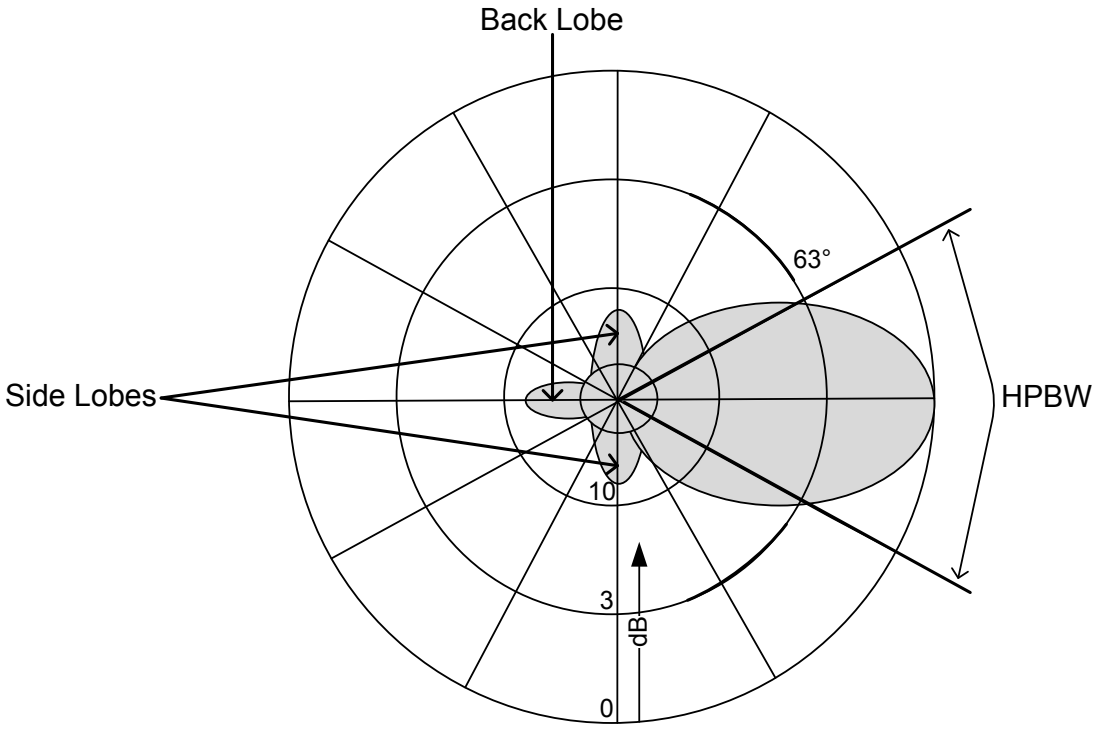

Figure 2-6: Radiation pattern of a generic antenna

Some common parameters used to compare radiation patterns are defined as follows:

- The half-power beamwidth (HPBW), or commonly the beamdwidth defines the aperture of the antenna. It is defined by the points in the horizontal and vertical beam patterns, which show where the radiated power has reached a -3dB level with respect to the main radiation direction. These points are also called 3 dB points.
- The front-back ratio is the ratio between the peak amplitudes of the main and back lobes, usually expressed in decibels.
- The sidelobe level is the amplitude of the biggest sidelobe, usually expressed in decibels relative to the peak of the main lobe [26].

2.2.1.4 Directivity

The directivity of an antenna $D(\theta,\phi)$, is a measure of the concentration of the radiated power in a particular θ,ϕ direction at a fixed distance *r* away from the antenna [18]. $D(\theta,\phi)$ is a function of the shape of the antenna pattern. It is the ratio of the radiation

intensity $U(\theta,\phi)$ in a given direction from the antenna to the radiation intensity averaged over all directions. The average radiation intensity in turn is equal to the total power radiated P_{rad} by the antenna over 4π [44]. Therefore, $D(\theta,\phi)$ is expressed as:

$$D(\theta,\phi) = \frac{4\pi U(\theta,\phi)}{P_{rad}} \tag{2-7}$$

The directivity of an antenna is often stated for an antenna as a number, which is in the direction of a maximum:

$$D_{\max} = \frac{U_{\max}}{U_{av}} \tag{2-8}$$

2.2.1.5 Gain

Gain refers to the amount of power radiated by an antenna in a specific direction relative to an ideal standard. The ideal standard is typically either a theoretical isotropic radiator (gain specified in dBi) or a free space half wavelength ($\lambda/2$) dipole (gain specified in dBd). The isotropic radiator has also an omnidirectional radiation characteristic in the E-plane and H-plane. The half-wave dipole is an antenna which is center-fed as to have equal current distribution in both halves. A free space dipole is defined to have 2.15 dB of gain relative to an isotropic radiator [23]. The gain is therefore defined as

Gain (reference to the isotropic radiator dBi) = Gain (referenced to λ/2-Dipole dBd) + 2.15dB (2-9)

The greater the gain is of the antenna, the narrower is its vertical-plane beamwidth. A high gain antenna will generally be of larger size. This is due to the greater number of dipole array and electrical elements required to reach this desired gain. Also, it is to note that doubling the antenna height causes a gain increase of 6 dB. However increasing the height also increases the transmission line losses and possible creation of nulls near the site [24].

2.2.1.6 Efficiency

Power in the antenna may be dissipated due to conductor loss or dielectric loss. Hence, antenna efficiency e can be defined as the ratio of total power radiated P_{rad} by the antenna to the input power P_{in} of the antenna:

$$e = \frac{P_{rad}}{P_{in}} \tag{2-10}$$

Note that $D(\theta,\phi)$ is a function of the shape of the antenna pattern and gain $G(\theta,\phi)$ takes into account the losses of the antenna. Then, the gain is related to the directivity as

$$G(\theta,\phi) = eD(\theta,\phi) \tag{2-11}$$

2.2.1.7 Voltage Standing Wave Ratio

If the source impedance $Z_S = R_S + jX_S$, where R_S is the source resistance, X_S is source reactance, and, the total antenna impendence, $Z_A = R_R + R_L + jX_A$, where R_R is the radiation resistance, R_L is the loss resistance, X_A is the antenna reactance, are complex conjugates, then the source is matched to the antenna [26]. Therefore, the maximum of the source power is delivered to the antenna. If the match is not ideal, then the degree of mismatch can be measured by the voltage standing wave ratio (VSWR), or by the reflection coefficient, Γ, defined by

$$\Gamma = \frac{V_R}{V_I} = \frac{Z_A - Z_S}{Z_A + Z_S} \tag{2-12}$$

where V_R and V_I are the amplitudes of the waves reflected from the antenna to the transmitter and incident from the transmitter onto the antenna terminals respectively.

Therefore, the VSWR is defined as

$$VSWR = \frac{1+|\Gamma|}{1-|\Gamma|}. \tag{2-13}$$

Commonly, antennas are designed to a standard input impedance of either 50Ω or 75Ω [26].

2.2.1.8 Bandwidth

The antenna's bandwidth specifies the frequency range over which it can properly radiate or receive energy. Precisely, the bandwidth is defined as the range over which the power gain is maintained to within 3dB of its maximum value, or the range over which the VSWR is no greater than 2:1, whichever is smaller [26]. The bandwidth is usually given as a percentage of the nominal operating frequency. Methods to compute the bandwidth are expressed in Equations (2-14) and (2-15). Narrowband antenna bandwidth is found as

$$BW = 100\left(\frac{F_H - F_L}{F_C}\right), \tag{2-14}$$

where F_H is the highest frequency in-band, F_L is the lowest frequency in-band and F_C is the center frequency of band. Broadband antenna bandwidth is expressed by the ratio

$$BW = \frac{F_H}{F_L}. \tag{2-15}$$

2.2.1.9 Scattering Parameters

Scattering Parameters (S-parameters) describe the reflection and transmission between the incident and reflection waves. These parameters relate to the travelling waves when a network is inserted into a transmission media. Scattering parameters represent the linear behavior of the two ports:

$\begin{bmatrix} |b_1|^2 \\ |b_2|^2 \end{bmatrix} = \begin{bmatrix} |s_{11}|^2 & |s_{12}|^2 \\ |s_{21}|^2 & |s_{22}|^2 \end{bmatrix} \begin{bmatrix} |a_1|^2 \\ |a_2|^2 \end{bmatrix}$, where $|b_i|^2$ and $|a_i|^2$ are the powered waves travelling towards and back from the 2-ports gate, respectively. $|s_{11}|^2$ is the reflected power from the first port, $|s_{12}|^2$ is the transmitted power from the first port to the second port, $|s_{22}|^2$ is the reflected power from the second port and $|s_{21}|^2$ is the transmitted power from the second port to the first port.

Insertion loss (*IL*) and return loss (*RL*) are also important parameters that may be extracted from S-parameters. Their descriptions follow.

The *IL* is defined as the loss of signal power resulting from the insertion of a device in a transmission line or optical fiber and is usually expressed in decibels (dB). In case the two measurement ports use the same reference impedance, *IL* is the dB expression of the transmission coefficient $|s_{21}|$ [64]. It is thus given by

$$IL = -20\log_{10}|s_{21}|. \tag{2-16}$$

The *RL* is a positive scalar quantity. The linear part, $|s_{11}|$ is equivalent to the reflected voltage magnitude divided by the incident voltage magnitude [60].

Input RL (RL_{in}) is a scalar measure of how close the actual input impedance of the network is to the nominal system impedance value and, expressed in logarithmic magnitude, is given by

$$RL_{in} = 20\log_{10}|s_{11}|. \tag{2-17}$$

Output return loss (RL_{out}) has a similar definition to the input return loss but applies to the output port (port 2) instead of the input port [60]. It is given by

$$RL_{out} = \left|20\log_{10}|s_{22}|\right|. \tag{2-18}$$

2.2.2 Transmission Schemes in LTE and LTE-Advanced

2.2.2.1 Smart Antennas

The definition of smart antennas is derived from [27, 28]. A smart antenna system combines multiple antenna elements with a signal processing capability to optimize its radiation and/or reception pattern automatically in response to the signal environment. Smart antenna systems are categorized as either switched-beam or adaptive-array systems.

Switched-beam implies the formation of multiple beams with heightened sensitivity depending on the directions. Based on the signal strength, these antenna systems choose from one of several predetermined, fixed beams, and switch from one beam to another as the mobile moves throughout the sector. Switched beam systems combine the outputs of multiple antennas in such a way as to form finely sectorized (directional) beams with more spatial selectivity than can be achieved with conventional, single-element approaches.

Adaptive array systems use a variety of signal-processing algorithms to effectively locate and track various types of signals, dynamically minimize interference and maximize intended signal reception.

2.2.2.2 Diversity

The basic concept of diversity is that the receiver should have available more than one version of the transmitted signal, where each version is received through a distinct channel. The impact from a deep fade (and hence loss of communication) is thus reduced.

Two major impairments can limit the performance and capacity of wireless communication systems: multipath fading and co-channel interference. Multipath fading is caused by multiple paths that the transmitted signal takes to the receive antenna. The signals from these paths add with different phases, resulting in a received signal amplitude and phase that vary with antenna location, direction and polarization as well as with time (with movement in the environment). Delay spread is the difference between the time of arrival of the earliest significant multipath component (typically the line-of-sight component) and the time of arrival of the latest multipath component. When the delay spread exceeds about 10 percent of the symbol duration, significant intersymbol interference can occur, which limits the maximum data rate. Co-channel interference results when cellular systems divide the available frequency channels into channel sets, using one channel set per cell, with frequency reuse, which increases as the number of channel sets decreases (i.e. as the capacity of each cell increases) [29]. It mainly results in the confusion in the tuning circuit of a wireless receiver due to a second wireless signal being detected with the same frequency.

The effective strength of the received signal can be increased via diversity. Two main methods are used:

- Switched diversity. Assuming that at least one antenna will be in a favorable location at a given moment, this system continually switches between antennas so as always to use the element with the highest signal power.
- Diversity combining. This approach corrects the phase error in two multipath signals and effectively combines the power of both signals to produce gain [29, 30].

2.2.2.3 Receive Diversity

This multi-antenna configuration is the use of multiple antennas at the receiver side. The basic principle consists of combining linear signals $r_1 \ldots r_{N_R}$ received at N_R different antennas. These received signals are multiplied by weight factors $w*_1 \ldots w*_{N_R}$ and added together, where "*" denotes a complex conjugate. The general vector notation of linear receive-antenna combining is expressed as

$$\hat{s} = [w*_1 \ldots w*_{N_R}] \cdot \begin{bmatrix} r_1 \\ \vdots \\ r_{N_R} \end{bmatrix} = \overline{w}^H \cdot \overline{r}. \tag{2-19}$$

The selection of the weight vector $\overline{w}$ differs depending on the specifics of antenna-combining approaches.

Provided radio-channel time dispersion does not occur, in other words, if the transmitted signal is only subject to non-frequency selective i.e. flat fading and white noise, the signals received at different antennas are

$$\overline{r} = \begin{bmatrix} r_1 \\ \vdots \\ r_{N_R} \end{bmatrix} = \begin{bmatrix} h_1 \\ \vdots \\ h_{N_R} \end{bmatrix} \cdot s + \begin{bmatrix} n_1 \\ \vdots \\ n_{N_R} \end{bmatrix} = \overline{h} \cdot s + \overline{n} \tag{2-20}$$

where s is the transmitted signal, vector $\overline{h}$ consists of N_R complex channel gains. Vector $\overline{n}$ consists of the noise impairing the signals received at different antennas.

After linear combining, in order to maximize the signal-to-noise ratio, the weight vector $\overline{w}$ should be selected as

$$\overline{w}_{MRC} = \overline{h}. \tag{2-21}$$

This combining method is known as Maximum-Ratio Combining (MRC). MRC does the following:

- Signals received at different antennas are phase rotated. This enables compensating for the corresponding channel phases and ensuring that the signals are aligned when added together.
- Signals in proportion to their corresponding channel gains are weighted. Higher weights are applied for stronger received signals.

2.2.2.4 Multiple Transmit Diversity

In downlink transmission i.e., from the BS to the UE, transmit diversity is an application implemented in LTE. In this scheme, the same data is sent from both antennas. The redundancy of the data in turn increases the robustness of the signal. Additional receive antennas and corresponding additional receiver chains are not necessarily needed when applying diversity and beam-forming with the use of multiple transmit antennas. In uplink transmission, the use of multiple transmit antennas increases complexity. It is thus preferred to apply additional receive antennas and corresponding receiver chains at the BS.

2.2.2.5 Delay Diversity

As the transmitted signal propagates to the receiver via multiple, independently fading paths with different delays, multi-path diversity or equivalently frequency diversity can be achieved. Radio-link performance may be improved from multi-path propagation with the assumption that Orthogonal Frequency Division Multiplexing (OFDM) transmission or advanced receiver-side equalization are used.

Time dispersion is the manifestation of multipath propagation stretching the signal in time so that the duration of the received signal is greater than the transmitted signal. Provided the channel is not time dispersive, the use of multiple transmit antennas can be used to create artificial time dispersion or equivalently creating artificial frequency selectivity by transmitting different relative delays from different antennas [31]. Figure 2-7 illustrates delay diversity in the case of two transmit (Tx) and one receive (Rx) antennas where the relative delay T should be selected to ensure suitable amount of frequency selectivity over the bandwidth of the signal to be transmitted. With different relative delays for each antenna, delay diversity can be extended to more than two antennas.

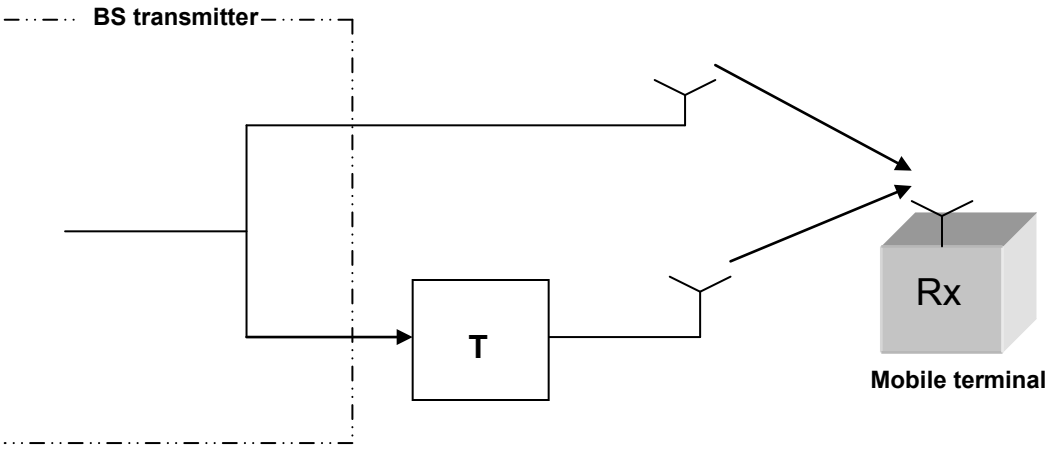

Figure 2-7: Two-antenna delay diversity

2.2.2.6 Transmitter-Side Beam-forming

Beamforming in essence is the shaping of the overall antenna beam in the direction of a target receiver. If some knowledge of the relative channel phases of the different antennas is available at the transmitter side, beamforming can be achieved. The signal strength at the receiver then increases in proportion to the number of transmitter antennas. Cases of high and low mutual correlation are considered in the following paragraphs.

An antenna configuration with a small inter-antenna distance defines high mutual antenna correlation. In this case, the overall transmission beam can be steered in different directions by applying different phase shifts to the signals to be transmitted on the different antennas. As the antenna distance is small, the overall transmission beam is relatively wide and adjustments of the antenna phase shifts. This is also referred to as classical beamforming. In classical beamforming, the signals to be transmitted on the different antennas are multiplied by different complex weights. This scheme is however limited to an increase of the received signal strength, it can not provide diversity.

Different antenna polarizations or large inter-antenna distance defines low mutual antenna correlation. As classical beamforming, the complex weights are also multiplied in this case to the transmitted signals. However, the antenna weights take general complex values. This means that both the phase and the amplitude of the signals to be

transmitted on the different antennas can be adjusted. In other words, due to the low mutual antenna correlation, both the phase and the instantaneous gain of the channels of each antenna may differ. Comparing with high mutual antenna correlation, in the case of low mutual antenna correlation, there is a need for more detailed channel knowledge and estimates of the instantaneous channel fading. This in turn contributes in providing diversity against radio-channel fading [31].

2.2.2.7 Spatial Multiplexing

Spatial multiplexing (SM) is another MIMO technology where two or more unique radio signals are sent over different links, so each signal carries different digital information. Spectrum efficiency is a commonly used term in cellular networks. It is the optimized use of spectrum or bandwidth so that the maximum amount of data can be transmitted with the fewest transmission errors. Spectrum efficiency equates to the maximum number of users per cell that can be provided while maintaining an acceptable quality of service (QoS). LTE-Advanced aims to increase and support a downlink peak spectrum efficiency of more than 15bps/Hz for eight antennas (MIMO 8x8) and an uplink spectrum efficiency above 7bps/Hz with four antennas (MIMO 4x4). Spatial division multiplexing (SDM) of multiple modulation symbol streams to both a single UE using the same time frequency resource, also referred to as Single-User MIMO (SU-MIMO) and to different UEs using the same time frequency resource, also referred to as Multi-User MIMO (MU-MIMO) are supported. In the uplink direction only MU-MIMO is used, i.e. there is only one modulated symbol stream per UE to be received by the NodeB, whereas multiple UEs may transmit on the same time frequency resource. The potential gain from MIMO and antenna beamforming is always a function of the number of antennas (columns). Higher order MIMO can benefit especially on peak and average data rates. Beamforming brings the most advantage on the cell edge. Multi beam processing may significantly enhance the performance in interference limited cells. Improvements can be achieved in terms of inter-cell interference, intracell interference, uplink imbalance and enhancements in the presence of multipath [32, 33].

2.2.2.8 Coordinated Multi-Point Transmission

Cooperation schemes generally have in common the forming of MU-MIMO or virtual MIMO systems. In the latter, antenna elements from different radio stations transmit simultaneously to UEs. In other words, CoMP schemes enable the dynamic coordination of transmission/reception at geographically separated points.

Two of the major categories of CoMP schemes discussed in LTE-A are joint processing and coordinated beamforming/scheduling.

In joint processing, multiple BSs jointly transmit signals to a mobile terminal, whereby signals from other cells turn from intercell interference into useful signals. This is mainly applicable for intersector cooperation, or intra-eNB cooperation.

Precoding is based on transmit beamforming concepts with the provision of allowing multiple beams to be simultaneously transmitted in the MIMO system. The LTE specification defines a set of complex weighting matrices for combining the layers before transmission using various antenna configurations. In coordinated beamforming and/or scheduling, BSs jointly choose precoding matrices, not only matching to their own serving terminals' channels but also less interfering to terminals scheduled in adjacent cells. This scheme may be suitable for inter-eNB cooperation [57].

3 CRLH LWAs

This chapter begins with an introduction to left-handed metamaterials. The transmission line model permitting CRLH structures is theorized. LWAs are described to progress on CRLH LWAs. Beam scanning methods using CRLH LWAs are described. In particular, frequency-scanned and varactor-controlled methods are reviewed.

3.1 Left-Handed Materials

Left-handed (LH) metamaterials (MTMs) are defined as artificial materials consisting of sub-wavelength unit cells arrayed in periodic structures. In the 1960s, a Russian physicist named Victor Vaselago analyzed a homogeneous medium in which both dielectric permittivity ε and magnetic permeability μ were negative [34]. This resulted in a negative refractive index (NRI). Vaselago concluded that the direction of an electromagnetic (EM) wave's phase velocity would be opposite to the forward propagation of the wave's energy velocity. In fact, in an NRI media, these backward waves would be characterized by antiparallel phase and group velocities or the formation of a left-handed triplet by the wave vector, the electric field vector and the magnetic field [35].

Vaselago's description of this promising phenomena progressed only in 2000 when D. Smith and collaborators offered the first demonstration of a LH MTM consisting of metallic wires and split-ring resonators (SRR) [36]. Transmission line (TL) structures exhibiting strong LH medium properties soon followed SRR structures. This is the focus of the next section.

3.2 CRLH Transmission Line

MTMs are broadly defined as effectively homogeneous structures. A particular structure has its structural average cell size p much smaller than the guided wavelength λg. An average cell size should be at least smaller than a quarter of wavelength, $p < \lambda g/4$. The condition $p = \lambda g/4$ follows the definition from Caloz *et al.* in [9] and is referred to as the effective homogeneity limit or effective-homogeneity condition.

Figures 3-1(a), 3-1(b) and 3-1(c) depict respectively a purely right-handed (PRH), a purely left-handed (PLH) and a CRLH lossless TL structures. Figure 3-1(a)'s PRH TL is the combination of a per-unit length series inductance L'_R, per-unit length shunt capacitance C'_R. Figure 3-1(b) shows the PLH TL with its per-unit length series capacitance C'_L and per-unit length shunt inductance L'_L [37]. As a wave propagates along the structures, the associated currents and voltages induce other natural effects. As currents flow along C_L, magnetic fluxes are induced and therefore a series inductance L_R is also present; in addition, voltage gradients exist between the upper conductors and the ground plane, which corresponds to a shunt capacitance C_R. As a consequence, the PLH structure in Figure 3-1(b) does not exist, even in a restricted frequency range, since a real LH structure necessarily includes (L_R, C_R) contributions in addition to the (L_L, C_L) reactances. Hence the motivation for the introduction of the term "composite right/left-handed" (CRLH), allowing to account for the exact nature of practical LH media [9]. Figure 3-1(c) consists of a capacitance C_L in series with an inductance L_R and a shunt capacitance C_R in parallel to an inductance L_L.

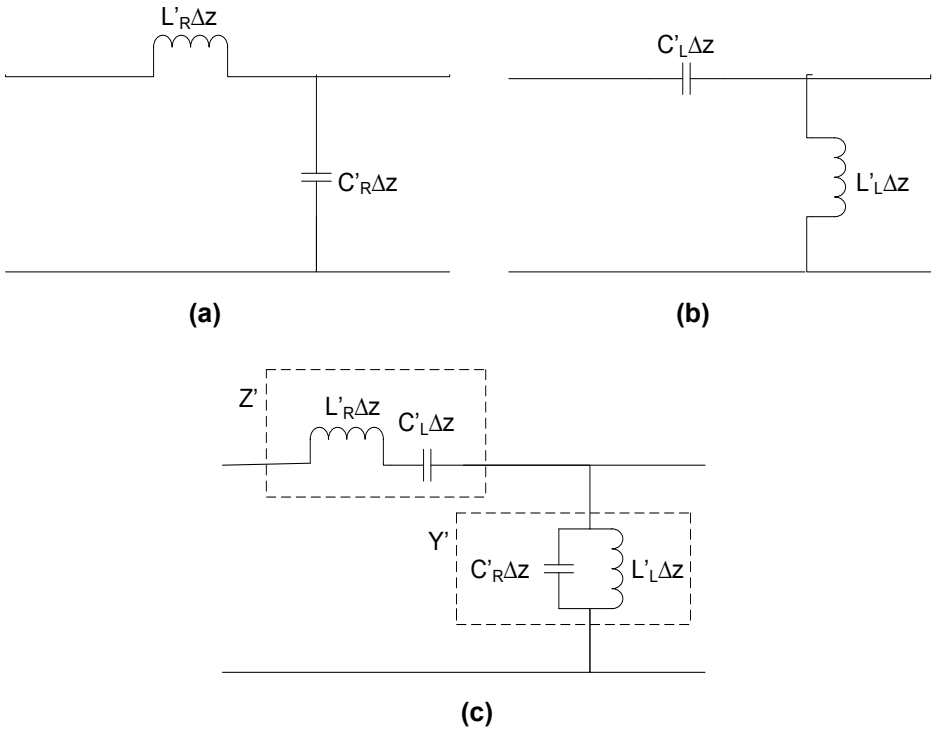

Figure 3-1: Transmissions lines: (a) RH homogeneous TL (b) LH homogeneous TL (c) CRLH TL

At low frequencies, L_R and C_R have tendency in being short and open, respectively. This reduces Figure 3-1(c) to the series C_L and shunt L_L. The circuit then exhibits LH properties with antiparallel phase and group velocities. It is also of highpass nature. This implies that a RH stopband is present above a certain cutoff. In general, the shunt resonance ω_{sh} is different from the series resonance ω_{se}. Provided these resonances are to be made equal i.e. balanced, this gap disappears. From that case, Figure 3-2 shows a transition frequency ω_o where an infinite-wavelength $\lambda g = 2\pi/|\beta|$ propagation is achieved. Also shown in this figure are the curves for a PLH structure ($L_R = C_R = 0$) and for a PRH structure ($L_L = C_L = \infty$). This figure represents the case $\omega_{se} < \omega_{sh}$, but $\omega_{se} > \omega_{sh}$ is also possible, depending on the LC parameters.

Although it has filter characteristics, the CRLH structure is never operated at the edges of the Brillouin zone, where $p \approx \lambda g/2$. It is operated only at the vicinity as effective-homogeneity ($p < \lambda g/4$) is ensured. Another point to note is that due to the LH and RH combined effects at all frequencies, the CRLH structure's dispersion curve differs from the PLH and PRH structures in both the LH and RH ranges.

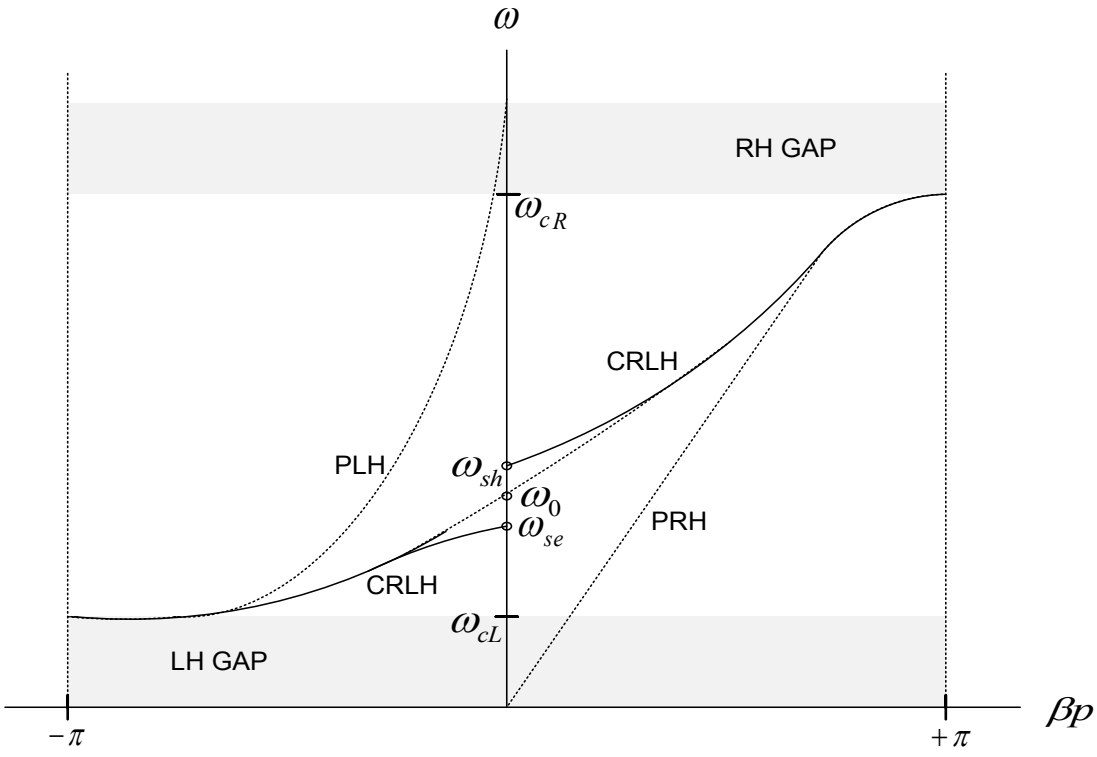

Figure 3-2: Dispersion diagram

Following the analysis presented in [37] and referring to Figure 3-1(c), consider the propagation constant of the TL given by $\gamma = \alpha + j\beta = \sqrt{Z'Y'}$, where Z' and Y' are, respectively the per-unit length impedance and per-unit length admittance. For the CRLH TL case, Z' and Y' are defined as

$$\begin{aligned} Z'(\omega) &= j(\omega L'_R - \frac{1}{\omega C'_L}), \\ Y'(\omega) &= j(\omega C'_R - \frac{1}{\omega L'_L}). \end{aligned} \tag{3-1}$$

The dispersion relation for a CRLH TL is

$$\beta(\omega) = s(\omega)\sqrt{\omega^2 L'_R C'_R + \frac{1}{\omega^2 L'_L C'_L} - \left(\frac{L'_R}{L'_R} + \frac{C'_R}{C'_L}\right)}, \tag{3-2}$$

where

$$s(\omega) = \begin{cases} -1 & if\ \omega < \omega_{\Gamma 1} = \min\left(\frac{1}{\sqrt{L'_R C'_L}}, \frac{1}{\sqrt{L'_L C'_E}}\right) \\ +1 & if\ \omega > \omega_{\Gamma 2} = \max\left(\frac{1}{\sqrt{L'_R C'_L}}, \frac{1}{\sqrt{L'_L C'_E}}\right). \end{cases} \tag{3-3}$$

From Equation (3-3), depending on whether the radicand is positive or negative, the phase constant β can be purely real or purely imaginary, respectively. A stop-band occurs in the frequency range where β is purely imaginary since $\gamma = \alpha$. A pass-band is present where β is purely real, since $\gamma = j\beta$.

3.3 LWAs and CRLH LWAs

Leaky wave (LW) antennas (LWAs) have been subjected to study for over half a century. The benefit of high directivity without the need for complex feeding network holds for these antennas. A LWA is basically a waveguiding structure that possesses a mechanism that permits it to leak power all along its length [38]. Since LWAs are based on traveling waves, their size do not relate to the operating frequency, but to directivity [39]. LW structures are classified in two categories, uniform and periodic. This section briefs on these LW categories and their limitations. This is to motivate the use of MTM LW structures. An introduction is also provided on principles of electronic beam control.

3.3.1 Uniform LWAs

A uniform LW structure is a LW waveguide with either a cross section invariant along the direction of propagation or with a small and continuous variation (taper) of the cross section along the direction of propagation. In a uniform LWA, the dominant mode propagates i.e. the lowest-frequency fast-wave mode. For a conventional (PRH) LWA, only forward angles can be obtained since the propagation constant is greater than zero ($\beta > 0$) at all frequencies. Also, broadside radiation is not possible as it requires $\beta=0$, which occurs at DC [9].

Figure 3-3 illustrates a uniform LWA through a rectangular waveguide with longitudinal slot. The fundamental TE_{10} waveguide is a fast wave with the propagation constant defined as

$$\beta = \sqrt{k_o - (\frac{\pi}{a})^2}\ , \tag{3-4}$$

where k_o is the free space wave number ($= 2\pi/\lambda_o$). The radiation causes the wavenumber k_z of the propagation mode within the open waveguide structure to become complex. Applying concepts of the stationary-phase principle, it can be found that:

$$\frac{\beta}{k_o} = \frac{c}{v_{ph}} = \frac{\lambda_o}{\lambda_g} \approx \sin\theta_m \tag{3-5}$$

where c is the speed of light in free space, v_{ph} is the phase velocity, λ_g is the guide wavelength at the broadside frequency, θ_m is the angle of maximum radiation taken from broadside.

The expected behavior of the uniform LWA holds. The beam cannot be scanned too close to broadside ($\theta_m = 0$), since this corresponds to the cutoff frequency of the waveguide. Also, the beam cannot be scanned too close to endfire ($\theta_m = 90^o$). This would require the air-filled waveguide to operate at frequencies significantly above cutoff, where higher-order modes can propagate. Therefore, for a wave traveling in the positive z direction, scanning is limited to the forward quadrant only ($0 < \theta_m < \pi/2$) [40].

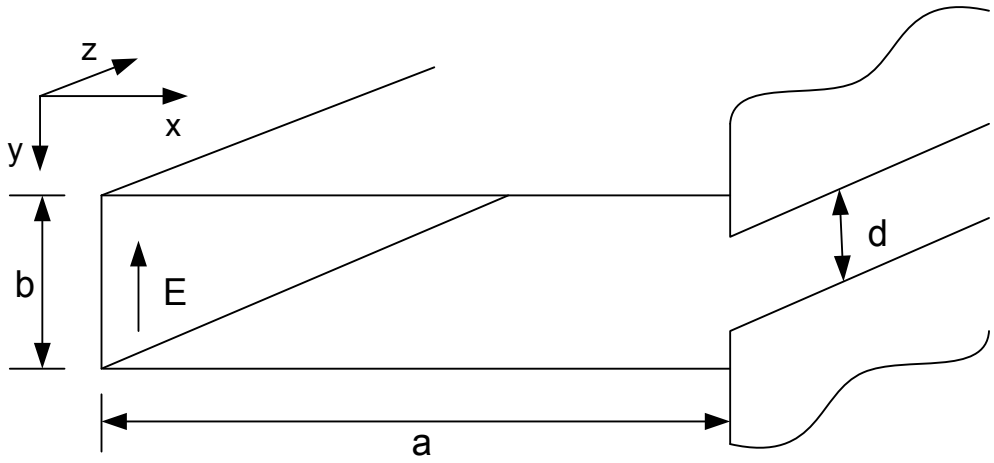

Figure 3-3: Slotted guide (patented by W. Hansen in 1940)

3.3.2 Periodic LWAs

A periodic LW structure is introduced by some periodic modulation. This periodicity produces leakage. The periodic modulation is uniform along the structure's length with the exception of small taper of the periodic properties along the length to control the sidelobes. This is turn implies a slow (non radiating) wave has been periodically modulated in some fashion. Since a slow wave radiates at discontinuities, the periodic modulations (discontinuities) cause the wave to radiate continuously along the length of the structure. Thus, the periodic modulation creates a guided wave that consists of an infinite number of space harmonics (Floquet modes). Although the main (n = 0) space harmonic is a slow wave, one of the space harmonics (usually the n = −1) is designed to be a fast wave, and hence a radiating wave. In other words, periodic LW structures have a *slow wave/guided dominant mode* and their radiation can therefore be obtained only from the contribution of one or several *fast-wave space harmonics* to the total field [9, 40].

Figure 3-4's LWA is a dielectric rectangular rod on which a periodic array of metal is placed. The periodicity introduces an infinity of space harmonics, each characterized by a phase constant β_n and related to each other by

$$\beta_n p = \beta_o p + 2n\pi, \tag{3-6}$$

where p is the period and β_o, the fundamental space harmonic. Depending on the values taken by β_n, the space harmonics can be forward or backward in nature, and be slow or

fast. Since the structure is open, a space harmonic that is fast will radiate. The conditions for the fast space harmonic are: $\beta_n/k_o<1$ and $\beta_o/k_o>1$. Rewriting Equation 3-6,

$$\frac{\beta_n}{k_o}=\frac{\beta_o}{k_o}+\frac{2n\pi}{k_o d}=\frac{\beta_o}{k_o}+\frac{n\lambda_o}{d} \tag{3-7}$$

it is observed that $|\beta_n/k_o|$ can be less than unity if n is negative and λ_o/d is suitably chosen. In practice, since a single radiated beam is desired, n=-1 is chosen as mentioned in the previous paragraph. At lower frequencies, all the space harmonics are slow and there are no radiated beams. As the frequency reach a value for which n = -1, space harmonic first becomes fast, the radiating beam just emerges from backward end-fire. As the frequency increases, the beam swings up from backward end-fire but is still radiating into the backward quadrant. Further increases in the frequency will swing the beam toward broadside, then through broadside, and finally into the forward quadrant. The penetration in the forward quadrant is dependent on the antenna's properties, in this case, mainly the dielectric constant. The antenna is useful only if a single, controllable beam is radiated, and the range in the forward quadrant is usually limited by the emergence of the n = -2 beam from backward end-fire, or by the next waveguide mode coming above cutoff [38].

The systematic presence of a gap at β = 0 in conventional periodic structures prevents broadside radiation because the gap edges correspond to a Bragg resonance (vg = 0) associated with standing waves. The large VSWR resulting from this effect means that power is reflected back to the source rather than being radiated. Further, the presence of this gap prevents a continuous radiation from backward to forward angles because no radiation is possible over the extent of the gap. Finally, even if the gap is relatively small, switching from backward to forward angles requires switching from the excitation of a negative space harmonic to a positive space harmonic. This requirement may have very different modal field distributions and input impedances, causing problems of feeding. Therefore, in practice, a periodic LWA can radiate only in a restricted range of backward angles or in a restricted range of forward angles, with the exclusion of broadside [9].

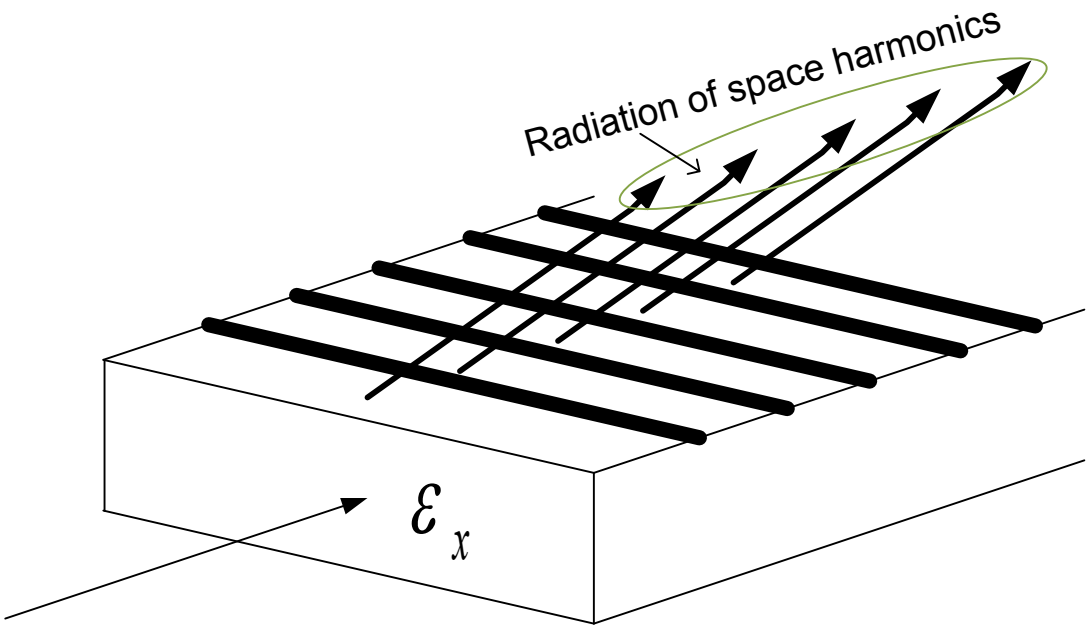

Figure 3-4: A rectangular dielectric rod on which is placed a periodic array of metal strips

3.3.3 Backfire to Endfire LWAs

The balanced CRLH-TL (discussed in section 3.2) can be used as a frequency-scanned LWA when matched to the air impedance. Referring to the dispersion diagram in Figure 3-2, if the CRLH structure is unbalanced, there is an additional gap region. This region is from $\min(\omega_{se}, \omega_{sh})$ to $\max(\omega_{se}, \omega_{sh})$ between the LH-leaky and RH-leaky regions. The gap is unfavorable for antennas because it prevents broadside radiation and introduces a gap in the scanning range.

In general, the CRLH LWA is structurally periodic. At this configuration, it can operate at its dominant mode. This is similar to the operation of uniform LWAs. The dominant mode contains a fast wave region and a guided region as shown in Figure 3-5(a). The transition frequency ω_o begin the fast-wave point since the phase velocity $v_P(\omega_o) = \infty$ from $\beta(\omega_o) = 0$. The dispersion relation for a balanced CRLH TL is represented by

$$\beta(\omega_o) = \frac{1}{p}\left(\omega\sqrt{L_R C_R} - \frac{1}{\omega\sqrt{L_L C_L}}\right). \tag{3-8}$$

The air lines $\omega = \pm kc$ delimit the radiation region in Figure 3-5(a). It also exhibits four distinct regions: the LH guided region, the LH-leaky region, the RH-leaky region, and the

RH-guided region. The CRLH LWA is capable of continuous scanning from backward (backfire) to forward (endfire) angles as depicted in Figure 3-5(b). The scanning angle is given by

$$\theta = \sin^{-1}\left(\frac{\beta_o + 2n\pi/p}{k_o}\right), \tag{3-9}$$

where n is the index of spatial harmonics, p is the period, β_o is the propagation constant of the fundamental mode and k_o is the free-space wavenumber. Backfire radiation is achieved at the frequency ω_{BF} where $\beta = -k_o$. Broadside radiation is achieved at the frequency ω_o when $\beta = 0$. Endfire radiation is achieved at the frequency ω_{EF} where $\beta = +k_o$.

The phase constant and impedance can be found using the immittances of Equation 3-1 by applying the Bloch-Floquet theorem to the unit cell of Figure 3-1(c). Under the *balanced* condition they are derived as

$$\gamma_B(\omega) = \frac{1}{p}\cosh^{-1}\left\{1 - \frac{1}{2}\left[\left(\frac{\omega}{\omega_R} - \frac{\omega_L}{\omega}\right)^2 + \delta\right]\right\} \overset{\gamma_{BP}\to 0}{\to} \beta(\omega) = \frac{\omega}{\omega_R} - \frac{\omega_L}{\omega}, \tag{3-10a}$$

$$Z_B(\omega) = Z_L\sqrt{1 - \frac{1}{4}\left[\left(\frac{\omega}{\omega_R} - \frac{\omega_L}{\omega}\right)^2 + \delta\right]} \overset{\gamma_{BP}\to 0}{\to} Z_C(\omega) = Z_L = Z_R, \tag{3-10b}$$

where the infinitesimal-limit results were obtained by Taylor series approximations [58]. From these expressions, $\omega_R = 1/\sqrt{L_R C_R}$, $\omega_L = 1/\sqrt{L_L C_L}$, $Z_L = \sqrt{L_L C_L}$, and δ is a loss term. When the structure is open to free-space, the characteristic impedance is independent of frequency. This implies that $Z_C = Z_L = Z_R$. This allows a broadband matching to a constant impedance (generally 50Ω) ports. The real part of the Bloch impedance, Z_B, is shown in Figure 3-6 for the *balanced* CRLH unit-cell. In this case, Z_B is a constant value in the pass-band.

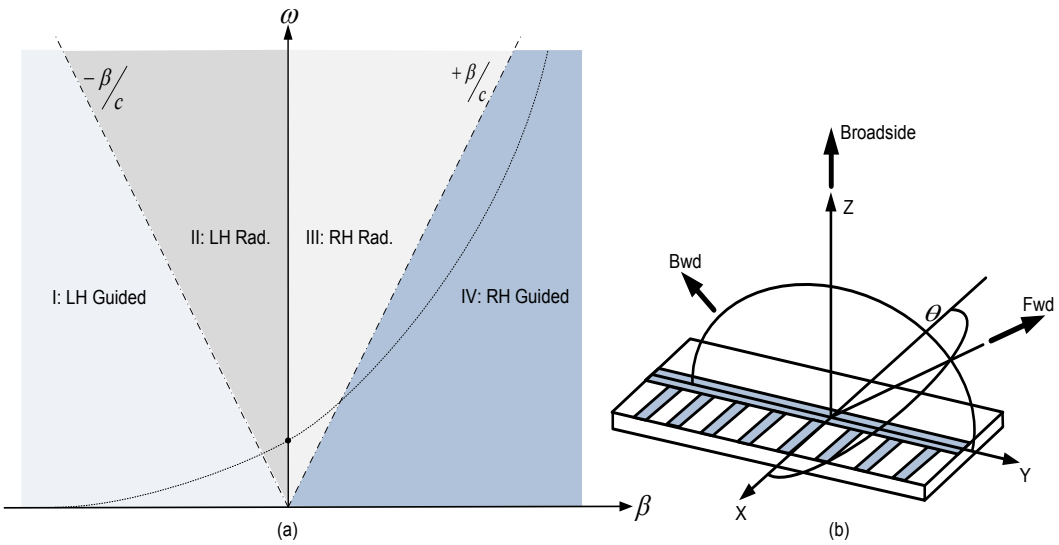

Figure 3-5: Balanced CRLH LWA: (a) Typical dispersion diagram (b) Scanning operation

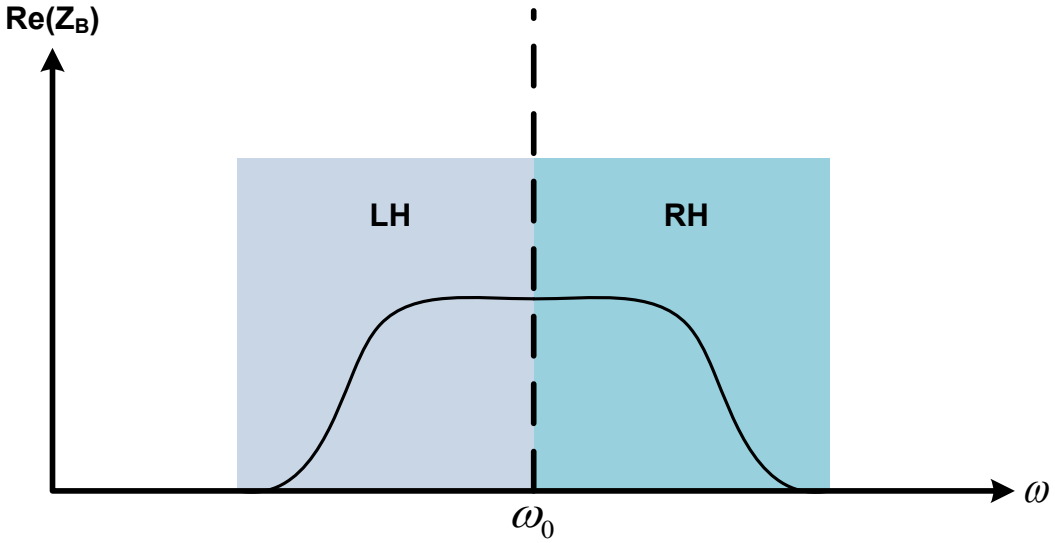

Figure 3-6: Bloch impedance diagram of unit-cell showing real part when $\omega_o = \omega_{se} = \omega_{sh}$

It is worth emphasizing the ability of broadside radiation for the balanced CRLH LWA. This antenna achieves broadside radiation as the group velocity $v_g = 0$ at $\beta = 0$. Uniform and periodic LWAs have this limitation. Conventional nonperiodic LWAs can scan from broadside to endfire, since β is positive. In addition, they can not radiate at broadside because $v_g = 0$ (standing wave) at $\beta = 0$. A periodic LWA is able to scan from backfire to endfire by operating at positive and negative space harmonics $(n = \pm 1, \pm 2, \ldots)$, though, broadside radiation can not occur [37].

3.3.4 Electronic Scanning and Beamwidth Control of LWAs

Section 3.3.3 reviewed that the scanning angle of CRLH LWAs is frequency-dependent, which is further expanded upon in chapter 4's design. For the sake of completeness on CRLH LWA theory, the electronic scanning method is also briefed upon in this section.

Investigations in [42] showed that by controlling the bias voltage of varactor diodes included in the CRLH unit cell, the capacitance of the cell can be changed. Thus, the propagation constant of the CRLH unit cell becomes a function of voltage. Since the voltage distribution applied to each cell can be different, a non-uniform voltage distribution can be realized. Depending on the type of voltage distribution, the antenna can be used as a scanning or beamwidth-controlling LWA.

3.3.4.1 Electronic Scanning

As described in 3.3.4, the angle of a CRLH LWA can be steered either by frequency tuning or by LC tuning at a fixed operation frequency. According to Equation 3-9, the main beam angle θ_{MB} of a LWA is a function of the propagation constant along the structure $\theta_{MB} = \theta_{MB}(\beta)$. In turn, the propagation constant depends on frequency and on LC parameters, $\beta = \beta(\omega; L_L; C_L; L_R; C_R)$. This can be observed from Equation 3-8.

The tuning of LC parameters is achieved by integrating varactor diodes in each cell of the CRLH structure. This enables controlling the reverse bias voltage by varying the capacitances. Therefore, the main beam angle is a function of voltage, $\theta_{MB} = \theta_{MB}(V)$. By varying the reverse bias voltages, which changes the values of C_L or C_R or both, the dispersion curve of Figure 3-5(a) is shifted in the ω - β plane and slightly altered in shape. Figure 3-7 illustrates this reasoning, representing three bias conditions.

So backfire-to-endfire electronic scanning is achieved if the value of β can be varied within a voltage range [V_{BF}, V_{EF}] from $\beta_{BF} = -\omega/c$ to $\beta_{EF} = +\omega/c$. Since ω_o does not correspond to the transition frequency for the other curves, the balanced structure is required as the dispersion curve crosses the frequency axis at ω_o, $\beta(V_o)$.

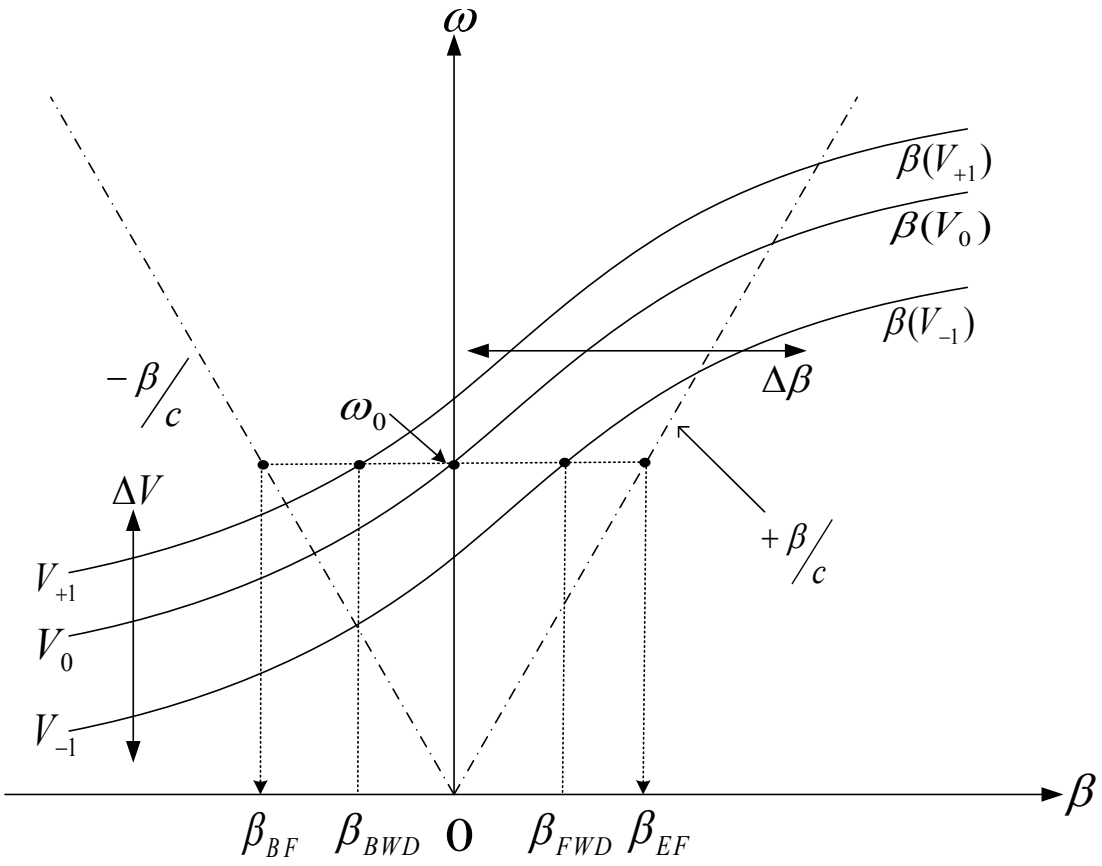

Figure 3-7: Different bias voltages yielding different values of θ_{MB} with the operation frequency fixed at f_o

If the bias voltage is the same for all cells in the CRLH structure (i.e. uniform), the LWA can be designed for maximum directivity. This is illustrated in Figure 3-8(a). As the cells have the same capacitance parameters, the structure is periodic. Also, since the unit cell of the structure is much smaller than the wavelength and radiating toward the same direction, the structure can be characterized as uniform [$\beta \neq \beta(z)$].

3.3.4.2 Electronic Beamwidth Control

Distributing different bias voltages from one cell to the other within the CRLH LWA yields a nonuniform structure [$\beta = \beta(z)$]. This is turn increases the beamwidth with the superposition of all the radiations as different cells radiate toward different angles. This is illustrated in Figure 3-8(b). Therefore, when the cells are nonuniformly biased, the antenna functions as an electronic beamwidth-controllable LWA. This is particularly useful for point-to-multipoint communications. Also, the concept does not require any corporate feeding network.

In [8], electronically-scanned CRLH LWAs were presented with varactor diodes at the LO. The LWAs were fed by a series uniform boxed CRLH power divider. This allowed an arbitrary number of antenna elements, which may be arbitrarily spaced, and the number of which may even be dynamically controlled for real-time beam shaping. Thus, the CRLH LWAs may be enabled to perform real-time scanning calibration to the scattering environment for channel maximization. The reader is directed to [10, 11] if the latter incites further interest.

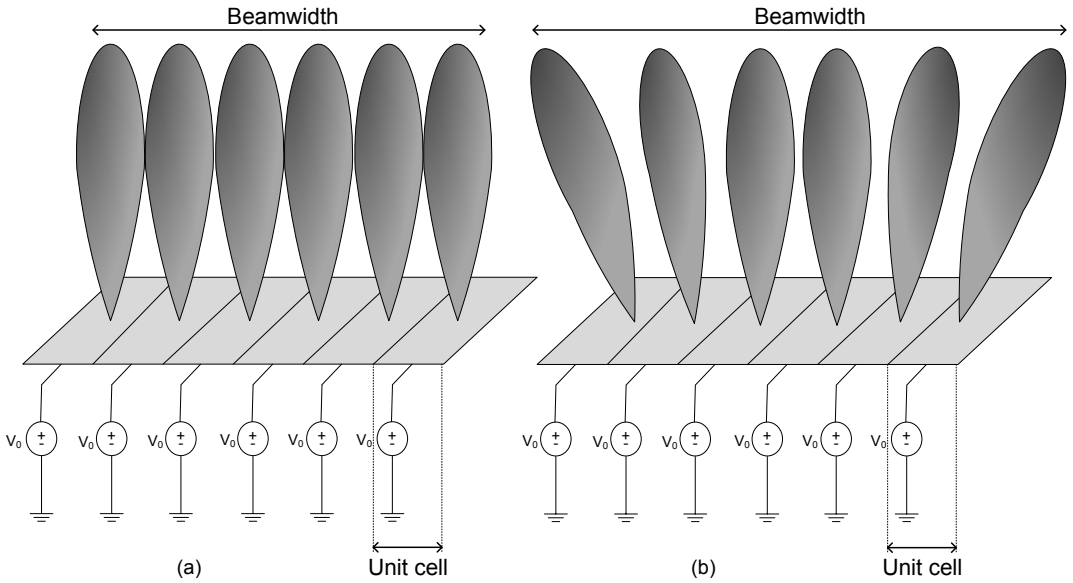

Figure 3-8: Beamwidth control principle: (a) Electronic scanning (b) Electronic beamwidth control

4 Design Specifications and Simulation Results

This chapter starts with the description of the antenna solution proposal and the justification for the antenna selection. It then provides design specifications on the conventional IDC and WBIDC CRLH unit cells and LWA with feed sections. The geometrical details of the latter are provided. The diagrams analyzed from simulation results with Ansoft Designer are documented. In particular, dispersion, *IL*, *RL* and the far field plot of the radiation pattern are considered. Antenna fabrication process with details on inputs required is discussed. A summary is provided on the work presented in this chapter.

4.1 Antenna Solution Proposal

Section 2.1 derived the vision of the CR enabled HeNB while section 2.2 elaborated on transmission schemes. In addition, factors like compactness, beam steering reconfigurability and relatively simple feeding mechanisms for the antennas are taken in consideration. A CRLH frequency-scanned LWA is known to address the previous sentence's statements. This CRLH LWA was introduced in section 1.2 and detailed in chapter 3. Transmission schemes with CRLH LWA and capacity analysis also demonstrated positive outcomes with DRPD in [10-11].

In general, CRLH LWAs are designed with IDC. The IDC structure can be easily built in microstrip technology. However, it has a major drawback. The impact is seen when wanting to obtain high capacitance values. In this case, many long thin fingers are needed, along with thin slots between them. When more than three fingers are used, resonances of the different modes arise in the multiconductor IDC structure. In a CRLH TL configured with IDC, those resonances occur and prevent the line from propagating any signal at these frequencies. In contrast, the so-called WBIDC overcomes this drawback by interconnecting the ends of the fingers on the same side of the IDC. This is done by means of bonding wires. This prevents all the modes of the multiconductor

structure from appearing, with the exception of the fundamental one. In consequence, the operational frequency range of the CRLH TL is significantly increased [61].
Therefore, the frequency-scanned WBIDC CRLH LWA is the proposed candidate in the CR enabled HeNB for this thesis. This MTM LWA will be used as a secondary integrated antenna in the femtocell BS. This means that it will support (say) an omni-directional antenna integrated with the HeNB which targets to cover the entire femtocell.

This idea can be further envisioned thinking about multi-band antenna architectures covering the same sector. A typical example can be a dual-band, dual-polarized, two column radome as described in [47]. The radome covers the same sector at two different bands and its elevation angle can be controlled by the same BS (if RET is applicable). The feeders connecting to the antenna ports for each column can connect to the same radios within the cabinet for different standards (i.e. multi-standard RBS). Or, it can connect to different radios in different cabinets depending on the eNB's capabilities and/or the operator's requirements.

So the WBIDC CRLH LWA will radiate azimuthally (from backfire-to-endfire) based on the geographical positioning of primary and/or secondary users. It will do so knowing the opportunistic carrier aggregation availabilities triggered by the CR enabled femtocell that is in cooperation with the neighboring sectors. The LTE Frequency Division Duplexing (FDD) and Time Division Duplexing (TDD) frequency bands are provided in Tables 4-1 and 4-2, respectively. This antenna will radiate with broadside on the DL in band 7.

The combination of band 7 (FDD) & band 38/40/41 (TDD) constitutes a single frequency range for 4G worldwide roaming and mass-market opportunity. RF front-end-module designs for unified common 2.3-2.7 GHz are supported by a large majority of RF component vendors. In fact, 2.3 to 2.7GHz is the only global band for 4G wireless technologies [65]. Hence justifies the reasoning behind designing the antenna in band 7.

Table 4-1: LTE FDD frequency bands

LTE band number	Uplink (MHz)	Downlink (MHz)
1	1920 – 1980	2110 – 2170
2	1850 – 1910	1930 – 1990
3	1710 – 1785	1805 – 1880
4	1710 – 1755	2110 – 2155
5	824 – 849	869 – 894
6	830 – 840	865 – 875
7	2500 – 2570	2620 – 2690
8	880 – 915	925 – 960
9	1749.9 – 1784.9	1844.9 – 1879.9
10	1710 – 1770	2110 – 2170
11	1427.9 – 1452.9	1475.9 – 1500.9
12	698 – 716	728 – 746
13	777 – 787	746 – 756
14	788 – 798	758 – 768
17	704 – 716	734 – 746
18	815 – 830	860 – 875
19	830 – 845	875 – 890
20	832 – 862	791 – 821
21	1447.9 – 1462.9	1495.5 – 1510.9
22	3410 – 3500	3510 – 3600

Table 4-2: LTE TDD frequency bands

LTE band number	Allocation (MHz)	Width of Band (MHz)
33	1900 - 1920	20
34	2010 - 2025	15
35	1850 - 1910	60
36	1930 - 1990	60
37	1910 - 1930	20
38	2570 - 2620	50
39	1880 - 1920	40
40	2300 - 2400	100
41	2496 - 2690	194

4.2 Design Specifications

Figure 4-1 illustrates the geometry of the one-dimensional CRLH conventional IDC unit-cell. Figure 4-2 illustrates the geometry of the WBIDC unit-cell. In both cases, the unit-cell is composed of series capacitors C_L and shunt (stub) inductors L_L. As currents flow through C_L, magnetic fluxes are induced and thus a series inductance L_R is also present. Also, voltage gradients exist between upper conductors and the ground plane, which corresponds to a shunt capacitance C_R [56]. Figure 4-2's WBIDCs design is made by placing short circuits at the end of alternate fingers of the IDCs. The antennas are printed on RT/Duroid 5880 with dielectric constant $\varepsilon_r = 2.2$ and thickness h = 1.57 mm. These laminates are selected as the dielectric constant is the lowest of the RT/Duroid products. Low dielectric losses make these laminates well suited for high frequency (WBIDC configured) application, where dispersion and losses need to be minimized. Also, these circuit materials are easily cut, sheared and machined to shape, and resistant to all solvents and reagents normally used in etching printed circuits or plating edges and holes. They have the lowest electrical loss of any reinforced Polytetrafluoroethylene (PTFE)

material, low moisture absorption, are isotropic, and have uniform electrical properties over frequency [63].

The simulation also considers a separate layer h' = 1.57 mm to account for the shorting of alternate fingers in the WBIDC case. Table 4-3 provides the values and descriptions of additional dimensions to complement Figures 4-1 and 4-2.

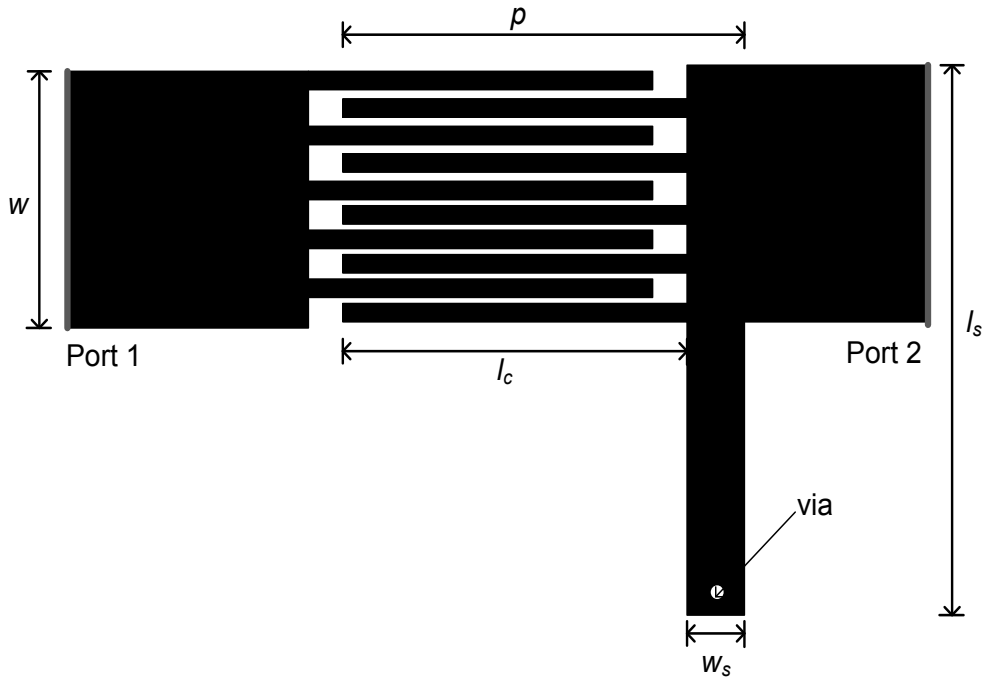

Figure 4-1: Conventional CRLH unit-cell

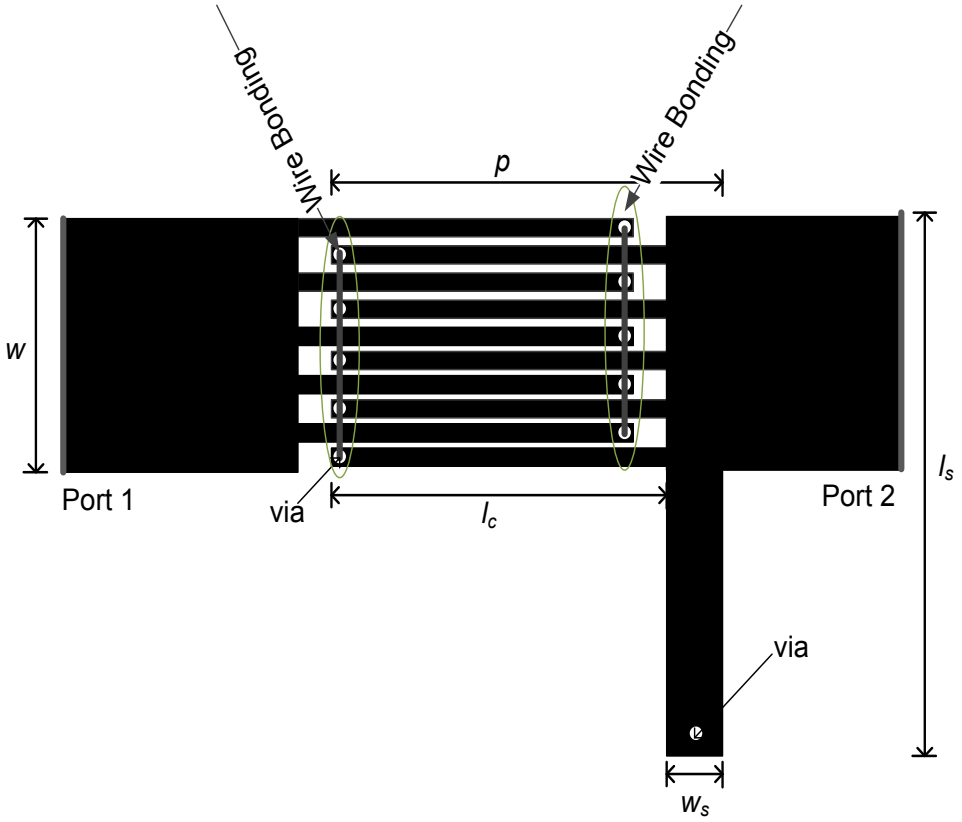

Figure 4-2: WBIDC CRLH unit-cell

Table 4-3: Unit-Cell Design Values

Variables		Value [mm]
Unit-cell period	p	12.2
Stub length	l_s	7.8
Stub width	w_s	1.0
Interdigital finger length	l_c	11.2
Interdigital finger width	w_c	0.269
Spacing between fingers	S	0.263
Via radius	R	0.12
Wire bonding via radius	R_w	0.1
Layer height	h	1.57

4.3 Simulation Results

The dispersion diagram in Figure 4-3 based on Table 4-3's design shows the leakage regions of the CRLH LWA without WBIDC. In comparison, Figure 4-4 shows the leakage regions for a WBIDC CRLH LWA. In both figures, included are backward leakage: 2.2 GHz < f_{LH} < 2.6 GHz, broadside leakage: f_o = 2.6 GHz and forward leakage: 2.6 GHz < f_{RH} < 3.25 GHz. Self-resonance suppression due to WBIDC design is clearly observed in Figure 4.4. In fact, the undesired resonances of the IDC, due to the multiconductor structure, are removed. This results when the bonding wires of the WBIDC are connected. Comparing to the IDC unit-cell, the WBIDC structure also extends significantly the frequency range of the CRLH TL in the higher frequencies, making the antenna rather flexible to CR applications.

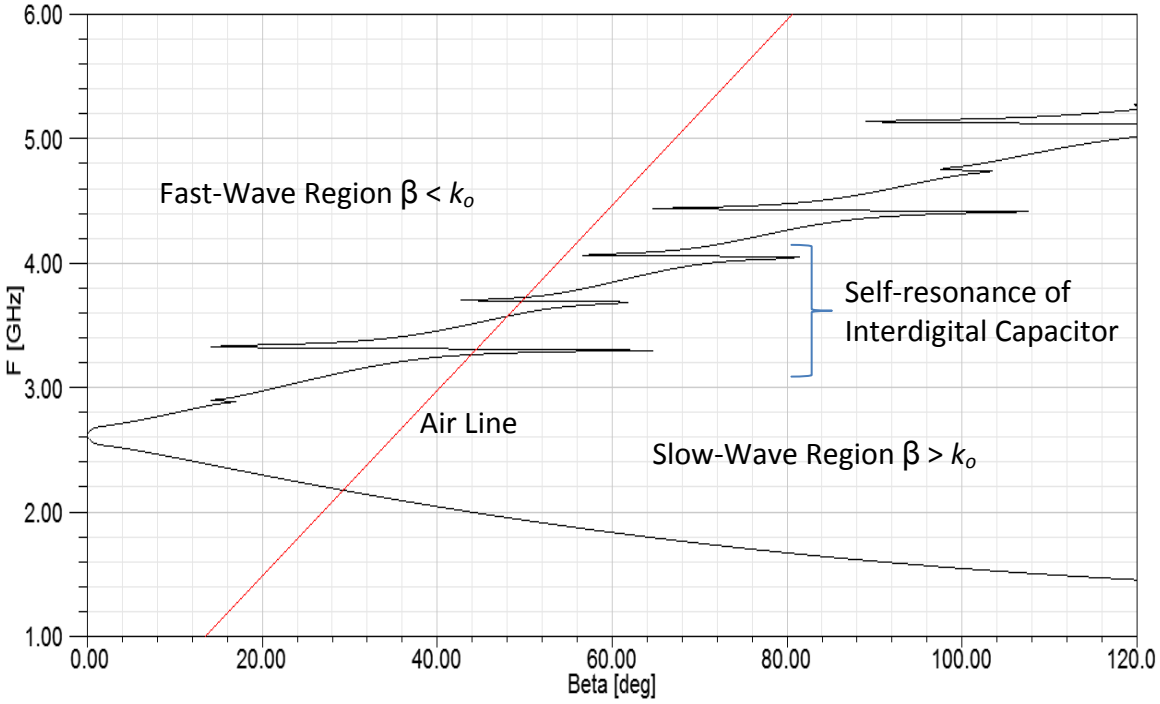

Figure 4-3: Dispersion diagram of the CRLH unit-cell

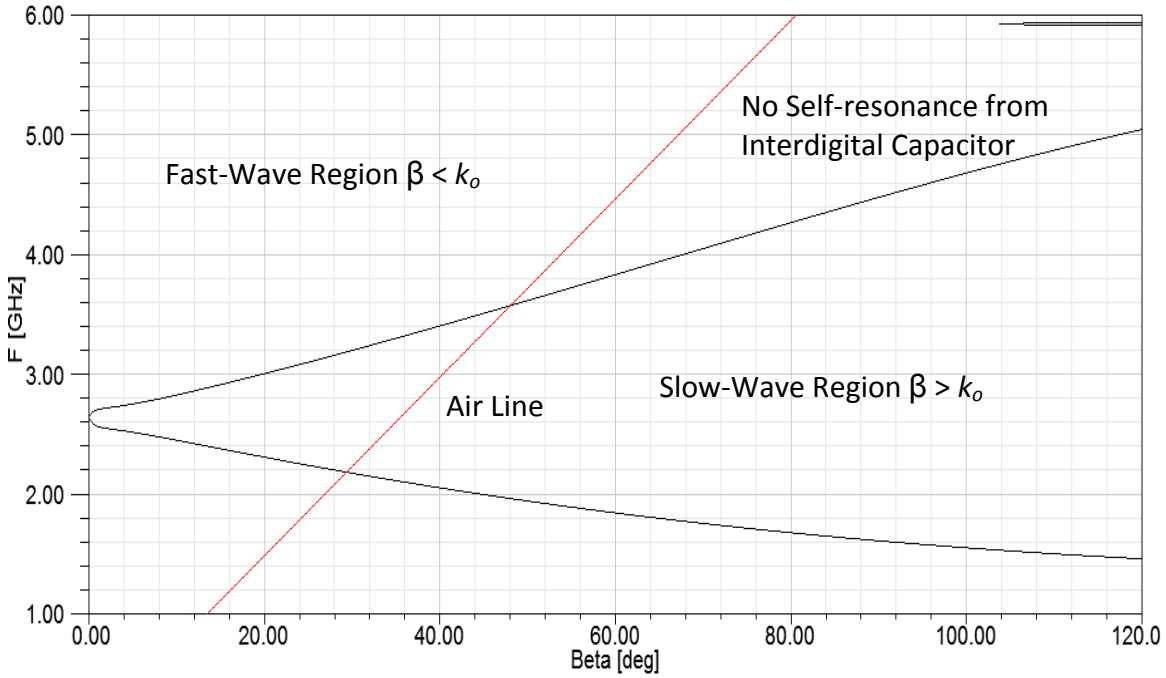

Figure 4-4: Dispersion diagram of the WBIDC CRLH unit-cell

The feed network is designed with the three unit cells which compose the WBIDC CRLH LWA system. This is required for discontinuity and impedance matching. An excitation of 0.0 mA current is setup at port 2. This causes port 2 to behave as an open circuit. The resulting (optimized) feed length is slightly over half the unit cell period and results as 6.4 mm. The prototype is displayed in Figure 4-5.

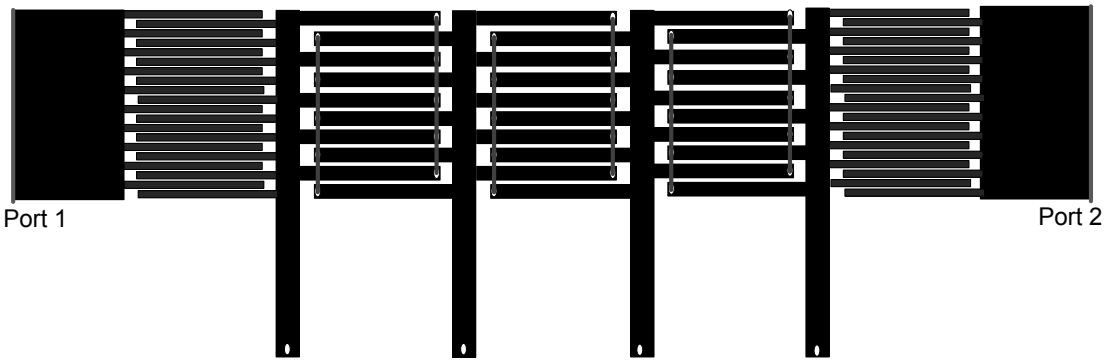

Figure 4-5: Prototype CRLH LWA consisting of three cascaded unit-cell with WBIDC

The resulting return (S_{11}) and insertion (S_{21}) loss is shown in Figure 4-6. The feed section was varied until the *RL* was around -8 to -10 dB for the majority of the fast-wave region. The *IL* does not exceed -3 dB for the majority of the leakage operation. Thus, the structure can radiate. Self-resonances from IDCs are also not observed due to the method of wire bonding.

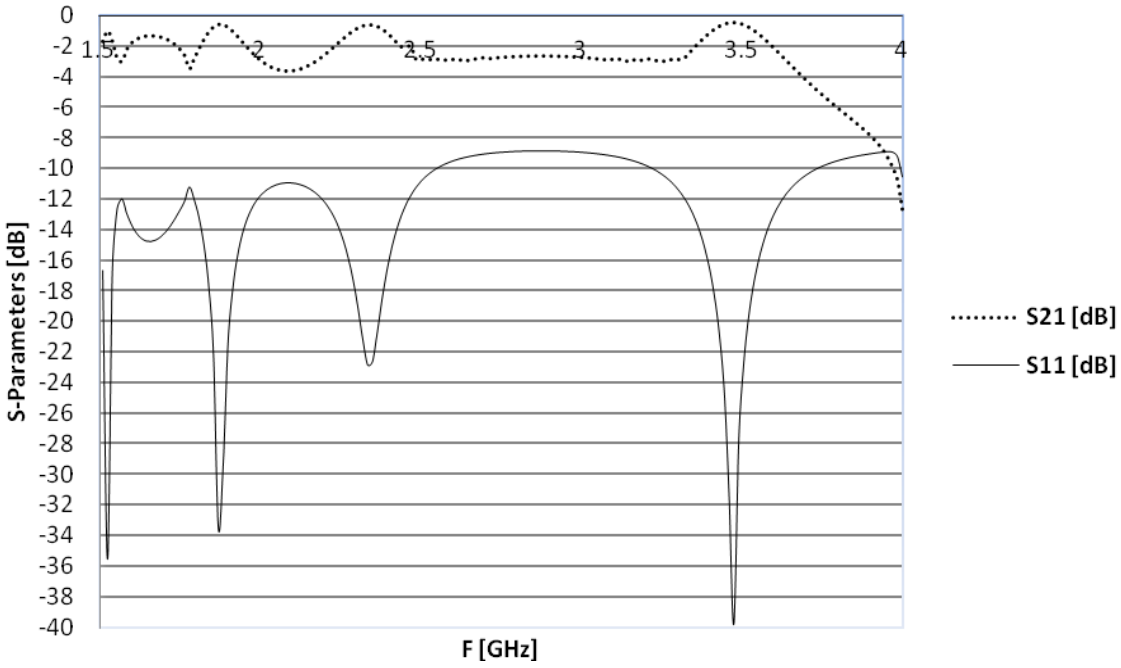

Figure 4-6: Insertion and return losses of three CRLH TL unit-cell with WBIDC

The far-field radiation patterns for three cascaded CRLH TL unit-cells are plotted with conventional IDCs in Figure 4-7 and WBIDCs in Figure 4-8. Figures 4-7 and 4-8 both confirm scanning capability of the CRLH LWA. Both designs have similar far-field plot patterns, with the endfire radiation having slightly higher gain in the case of WBIDC.

It can be seen that radiation pattern is backward from $-60 < \theta < 0$ degrees at 2.2 GHz, broadside at $\theta = 0$ degree at 2.6 GHz with a fan shape and forward as θ reaches upto 60 degrees at 3.25 GHz.

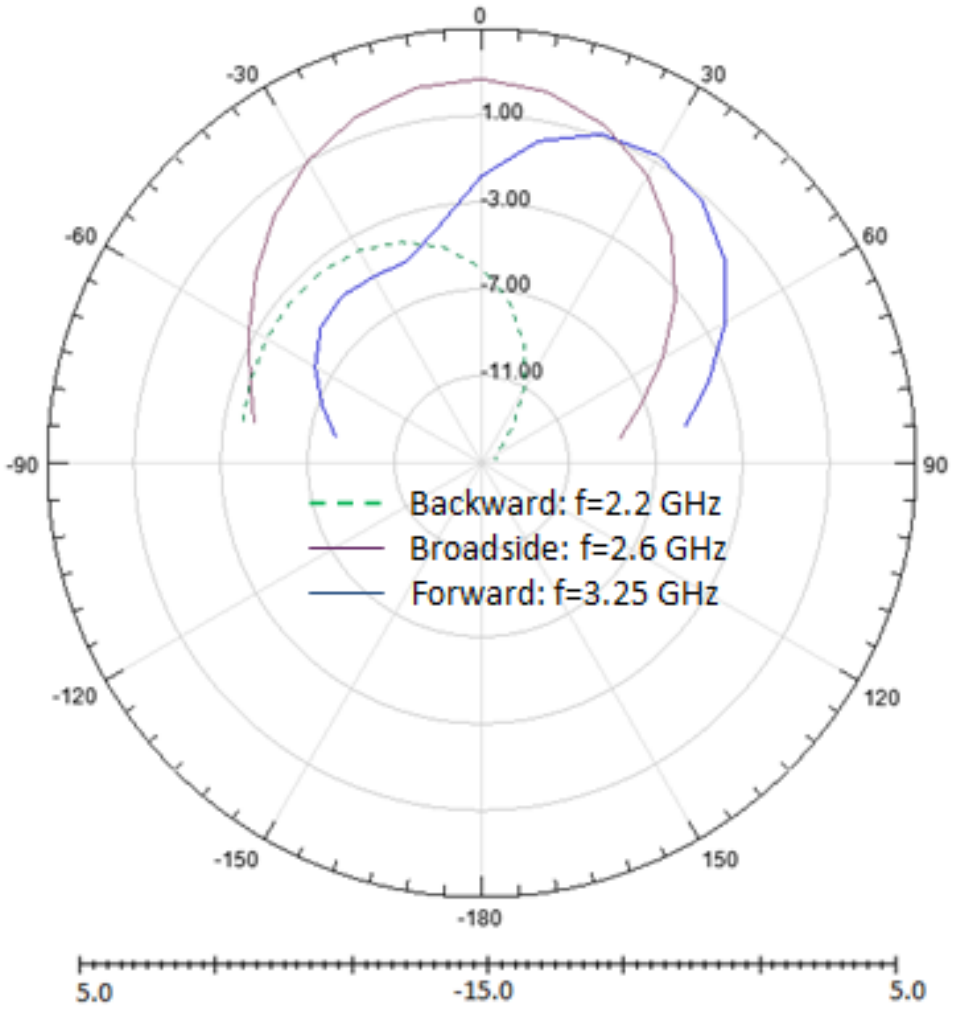

Figure 4-7: Far-field plot of three CRLH TL unit-cells

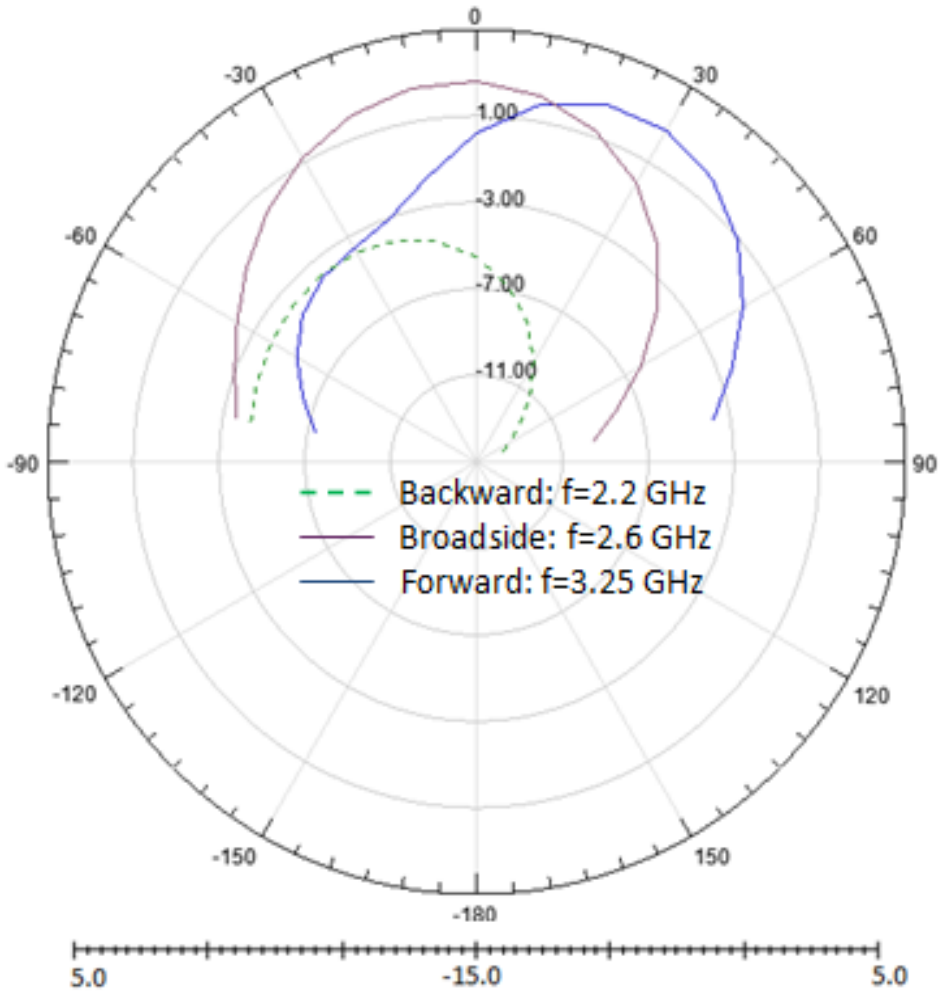

Figure 4-8: Far-field plot of three CRLH TL unit-cells with WBIDCs

4.4 Fabrication Process

This section provides details on inputs required from the Poly-Grames Research Center to take the simulated prototype into manufacturing and experimental validation. The Center is affiliated under École Polytechnique de Montréal, which in turn is a subset of the Université de Montréal.

The proposed antenna system is a multilayer CRLH LWA. It was designed with three-cascaded unit-cells with extra microstrip lines for port excitation. For multilayer fabrications, epoxy glue, high temperatures and pressure are used to combine the layers. The layers and final assembly are printed. The three-dimensional prototype of the antenna system is depicted in Figure 4-9.

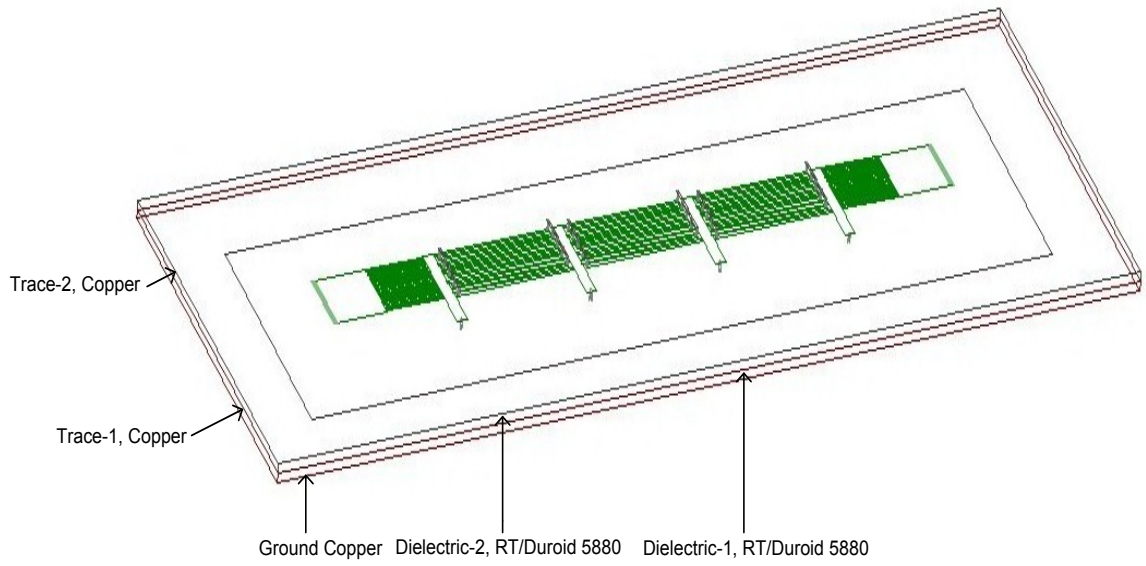

Figure 4-9: Three-dimensional prototype of three cascaded CRLH TL unit-cells with WBIDCs

The bottom layer is ground, consisting of copper material. The first dielectric is composed of Rogers RT/Duroid 5880. The periodic structure is then drawn on copper trace. The vias on the stubs terminate at ground. The vias on the IDCs terminate on the top layer trace. A second dielectric composed of Rogers RT/Duroid 5880 is between the periodic structure trace and the upper layer trace. Vias terminated on the upper copper trace are bonded with a thin metal strip. Metal strip instead of actual wires are recommended in the manufacturing as bonding with wires on copper is difficult and metal strip has greater robustness.
On the other hand, the conventional IDC prototype of Figure 4-1 is designed with the bottom layer consisting of copper material, the first dielectric composed of Rogers RT/Duroid 5880 and copper trace on the top layer for the antenna.
Applicable fields of the geometrical details of both IDC and WBIDC design structures can be found in Table 4-3.

In terms of inputs required for fabrication, each layer requires a Gerber formatted file. A photoplot file in Gerber format will essentially be used to create film. Photoplotters consists of a precision servo controlled X-Y table to which a piece of high contrast film is attached. A bright light source is directed through a shutter, through an aperture wheel and focused onto the film. A controller converts Gerber commands into the appropriate table movements, wheel rotation and shutter opening. As detailed in [12], the Gerber file is named in the following format: Name-substrate Number-layer .extension.

Drill file and vias require a drawing exchange format (.dxf) type file. This two-dimensional graphics file format is supported by virtually all PC-based Computer Aided Design (CAD) products. It was created by AutoDesk for the AutoCAD system. The data format of a DXF is called a "tagged data" format which means that each data element in the file is preceded by an integer number that is called a group code. A group code's value indicates what type of data element follows. This value also indicates the meaning of a data element for a given object (or record) type [62]. As detailed in [12], the drill file is also named in the following format: Name-substrate Number-layer .extension.

Rogers RT/Duroid 5880 laminates are ordered from http://www.rogerscorp.com/acm/ through the University Program form. A maximum of two samples are no-charge. Two panels of each sample are received. Two layers are composed of 5880 dielectric for the prototype. Rolled copper, 0.5 ounce thick (5R/5R) is provided at Poly-Grames. The fabrication time for the circuit is estimated at six man hours (mhrs).

4.5 Summary of Works Presented

Before concluding the thesis, this section enlists the presented work in this chapter.

1. An antenna system solution with the properties of CRLH LWA with WBIDC in a CR enabled HeNB for LTE-A was described.

2. Details were provided on how this antenna was envisioned to HeNBs (although frequency-scanned MTM based) with a realistic view of solution(s) that currently exist in deployments.

3. Justification of the antenna selection and reasoning behind the usage of WBIDC against IDC was explained.

4. Detailed design guidelines for the IDC and WBIDC CRLH LWAs in addition to the geometrical specifications were presented.

5. An antenna design respecting a commercial FDD band on the DL for LTE-A was successfully demonstrated through simulations.

6. Simulations also demonstrating the benefits of using WBIDC in CRLH LWA configurations in comparison to IDC were presented.

7. It was verified at the Poly-Grames Research Center that considering a separate layer with additional vias to account for the shorting of alternate fingers is more

practical and robust as a solution for wire bonding. In fact, it is known to be very difficult to bond on copper antenna and wire bonding in general is fragile. The length of wire bonding is not consistent and it is preferable to make the suggested via connections as mentioned in this thesis. Thus, the approach taken on this antenna's design makes it a more practical prototype for testing.

8. Manufacturing mhrs of the prototype system were also obtained from the research center based on layer-by-layer specs as part of the fabrication inputs.

5 Conclusion and Future Work

The main objective of this research was to propose and simulate an antenna system for an LTE-Advanced CR enabled HeNB in band 7 FDD. The usage of a frequency scanned CRLH LWA with WBIDC was justified for the latter. It was designed to radiate azimuthally (from backfire-to-endfire) from 2.2 to 3.25 GHz between -60 to 60 degrees. Broadside leakage occurred at 2.6 GHz. Thus, band 7's DL target was respected.

The antenna demonstrated full-scanning capability through frequency variation. It also benefited from the bonding of wires at higher frequencies. Self-resonances from IDCs were close to null in the wire bonded design in comparison to the IDC design. Far-field radiation pattern measurements were relatively similar in both IDC and WBIDC cases.

This MTM LWA was envisioned to be used as a secondary integrated antenna in the femtocell BS. It was projected to support (say) an omni-directional antenna integrated with the HeNB which targets to cover the entire femtocell. The CRLH LWA was mentioned to radiate based on the geographical positioning of primary and/or secondary users. It was proposed to do so by being informed of (through the BS's baseband) the opportunistic carrier aggregation availabilities triggered by the CR enabled HeNB that is in cooperation with the neighboring sectors.

Future work to accommodate the above paragraph will include further antenna design, investigation with LTE-A's over-the-air (OTA) features and system performance. For antenna design, voltage-scanned CRLH LWA with WBIDC can be compared to the frequency scanned WBIDC as an alternative. Power recycling mechanisms proposed in [55] can be investigated on the frequency and voltage scanned CRLH WBIDC structures. Both can also be experimentally demonstrated. For LTE-A OTA features and system performance, a vendor's prototype can be used to simulate the CR HeNB. Primary and secondary users (UEs) can be brought in to the serving cell and served by the secondary MTM antenna for capacity tests. DRPD can be investigated in conjunction with LTE-A features such as 4 x 2 transmission schemes, spectrum (carrier) aggregation and CoMP.

6 REFERENCES

[1] S. Parkvall, E. Dahlman, A. Furuskar, Y. Jading, M. Olsson, S. Wanstedt and K. Zangi, "LTE-Advanced – Evolving LTE towards IMT-Advanced," *Vehicular Technology Conference*, Fall-2008, pp. 1 – 5

[2] N. Manjaro and C. Gallen, *$8.6 Billion LTE Base Station Forecast Shows There Is Still Enthusiasm for Deployment*, ABI Research, New York, January 9 2009, [Online] Available: www.abiresearch.com

[3] A. Shukla, E. Burbidge and I. Usman, "Cognitive Radios – What are They and Why are the Military and Civil Users Interested in Them," *Antennas and Propagation, EuCAP*, Nov. 2007, pp. 1 – 10

[4] G. Scutari, D. Palomar and S. Barbarossa, "Cognitive MIMO radio," *IEEE Signal Processing Magazine*, Vol. 25, November 2008, pp. 46 – 59

[5] A. Furuskar, T. Jonsson and M. Lundevall, "The LTE radio interface – key characteristics and performance," *PIMRC 2008*, Sept. 2008, pp.1 – 5

[6] M.E. Ermutlu, "Meta materials in future wireless communication equipments," *Antennas and Propagation International Symposium,* June 2007, pp. 1164–1166

[7] J. Xiang, Y. Zhang, T. Skeie and X. Lang, "Downlink Spectrum Sharing for Cognitive Radio Femtocell Networks," *IEEE Systems Journal*, Vol. 4, 2010, pp. 524 – 534

[8] C. Caloz, T. Itoh and A. Rennings, "CRLH metamaterial leaky-wave and resonant antennas," *Antennas and Propagation Magazine*, Vol. 50, Oct. 2008, pp. 25 – 39

[9] C. Caloz and T. Itoh, *Electromagnetic Metamaterials: Transmission Line Theory and Microwave Applications*, John Wiley & Sons, New York, 2006

[10] J.-F. Frigon, C. Caloz and Z. Yanyang, "Dynamic radiation pattern diversity (DRPD) MIMO using CRLH leaky-wave antennas," *Radio and Wireless Symposium*, 2008, pp. 635 – 638

[11] X. Li and J-F. Frigon, Capacity Analysis of MIMO Systems with Dynamic Radiation Pattern Diversity, *Vehicular Technology Conference*, 2009, pp. 1 – 5

[12] Antonymous, *RF Circuit Fabrication Rules*, Poly-Grames, CREER, September 2011, [Online]
Available: http://www.creer.polymtl.ca/fr/ressources_files/fabrication_process

[13] A. Mihovska, F. Meucci, N.R. Prasad, F.J. Velez and O. Cabral, "Multi-operator resource sharing scenario in the context of IMT-Advanced systems," *CogART 2009*, May 2009, pp. 12 – 16

[14] M. Romney *et al.*, *LTE and the Evolution to 4G Wireless*, Agilent Technologies, China, 2009

[15] Anonymous, *WCDMA RAN Overview Solution Description*, Ericsson AB, April 2005, pp. 7

[16] T. Kitayabu, Y. Ikeda, Y. Amano and H. Ishikawa, "Concurrent Dual-Band Receiver for Spectrum Aggregation System," *RWS 2009*, Jan. 2009, pp. 634 – 637

[17] P. Olanders, "The com side of things," *EuMC 2009*, Oct. 2009, pp. 1059 – 1061

[18] P.R. Clayton, *Introduction to Electromagnetic Compatibility*, John Wiley & Sons, 2006

[19] P. Steenkiste *et al.*, "Future Directions in Cognitive Radio Network Research," *NSF Workshop Report*, March 9-10 2009, pp. 7

[20] Anonymous, *Single RAN made simple*, White paper, Nokia Siemens Networks, 2009, pp. 4
[21] C.G. Christodoulou, "Reconfigurable antennas in cognitive radio that can think for themselves?," *Microwave, Antenna, Propagation and EMC Technologies for Wireless Communications*, 2009
[22] J. Lyke, "Reconfigurable Systems: A Generalization of Reconfigurable Computational Strategies for Space Systems," *IEEE Aerospace Conference*, March 2002
[23] P. Scholz, *Basic Antenna Principles for Mobile Communications*, Kathrein-Werke KG, Rosenheim, 2001
[24] F.R. Connor, *Antennas*, London: Edward Arnold Publishing, 1989
[25] W. Gosling, *Radio Antennas and Propagation*, Woburn, MA: Newness Publishing, 1998
[26] S.R. Saunders, *Antennas and Propagation for Wireless Communication Systems*, Chichester: John Wiley and Sons INC., 1999, pp. 64
[27] Ng K. Chong, O. K. Leong, P. R. P. Hoole, and E. Gunawan, "Smart Antennas and Signal Processing," *WITPress 2001*, pp. 245 – 267
[28] Anonymous, *Smart Antenna Systems*, Web ProForum Tutorials, the International Engineering Consortium [Online] Available: http://www.iec.org
[29] I. Stevanovi, A. Skrivervik and J.R. Mosig, "Smart Antennas for Mobile Communications, " *Laboratoire d'Electromagnétisme et d'Acoustique*, Ecole Polytechnique Fédérale de Lausanne, 2003
[30] J. H. Winters, "Smart Antennas for Wireless Systems," *IEEE Personal Communications*, 1998, pp. 23 – 27
[31] E. Dahlman, S. Parkvall, J. Skold and P. Berming, *3G Evolution, HSPA and LTE for Mobile Broadband*, Burlington, MA : Elsevier LTd., 2008
[32] A. Ghosh, R. Ratasuk, B. Mondal, N. Mangalvedhe and T. Thomas, "LTE-Advanced: Next-Generation Wireless Broadband Technology," *Wireless Communications*, 2010, pp. 10 – 22
[33] V. Stencel, A. Muller and P. Frank, "LTE Advanced — A further evolutionary step for Next Generation Mobile Networks," *Radioelektronika, 20th International Conference*, 2010, pp. 1–5
[34] V. Veselago, "The electrodynamics of substances with simultaneously negative values of ε and μ," *Soviet Physics Uspekhi*, vol. 10, no. 4, Jan., Feb. 1968, pp. 509 – 514
[35] M. Stoytchev, A. Gummalla, M. Achour and G. Poilasne, "Beyond 3G: Metamaterials Application to the Air Interface," *Antennas and Propagation Society International Symposium*, 2007, pp. 1160 – 1163
[36] D. R. Smith, W. J. Padilla, D. C. Vier, S. C. Nemat-Nasser and S. Shultz, "Composite medium with simultaneously negative permeability and permittivity," *Phys. Rev. Lett.*, vol. 84, 2000, pp. 4184 – 4187
[37] A. Lai, C. Caloz and T. Itoh, "Composite right/left-handed transmission line metamaterials," *IEEE Microwave Magazine*, Sep. 2004, pp. 34 – 50
[38] A. Oliner and D. R. Jackson, "*Leaky-wave Antennas" in Antenna Engineering Handbook,* 4th Edition, McGraw-Hill, 2007
[39] M. A. Antoniades, *Microwave Devices and Antennas Based on Negative-Refractive-Index Transmission-Line Metamaterials*, Ph.D. Dissertation, University of Toronto, Dept. of Electrical Engineering, 2009

[40] F. Frezza, *Introduction to Traveling-Wave Antennas*, European School of Antennas, 1996, pp. 1 – 5
[41] Y. Hao and R. Mittra, *FDTD Modeling of Metamaterials Theory and Application*, Artech House, Massachusetts, 2009
[42] S. Lim, C. Caloz and T. Itoh, "Metamaterial-based electronically-controlled transmission line structure as a novel leaky-wave antenna with tunable radiation angle and beamwidth," *IEEE Trans. Microwave Theory Tech.*, vol. 53, no. 1, Nov. 2005, pp. 161 – 173
[43] F. Bilotti, A. Aluf, N. Engheta and L. Vegni, "Leaky-Wave Metamaterial Antennas: Conical and Pencil Beam Radiation," *Antennas and Propagation, EuCAP 2007*, pp. 1 – 5
[44] O. Nilmaz, *Self-Optimization of Coverage and Capacity in LTE using Adaptive Antenna Systems*, MSc thesis, Aalto University, February 2010
[45] J. Mitola, *Cognitive Radio An Integrated Agent Architecture for Software Defined Radio*, PhD thesis, KTH, May 2000
[46] M. Simsek, T. Akbudak, B. Zhao and A. Czylwik, "An LTE-Femtocell Dynamic System Level Simulator," *WSA 2010*, pp. 66 – 71
[47] V. Chandrashekhar and J. Andrews, "Femtocell Networks: A Survey," *IEEE Communications Magazine*, vol. 46, no. 9, Sept. 2008, pp. 59 – 67
[48] Anonymous, *MIMO and Smart Antennas for 3G and 4G Wireless Systems,* 3G Americas, May 2010
[49] Anonymous, *Mobile Communication Antennas*, Kathrein and Scholz, July 2001
[50] H. Huang, K. Lin, H. Su, C. Wu and H. Lin, "Design of dual-polarized high-gain antenna radome by using Jerusalem cross metamaterial structure," *APSURSI '09*, pp. 1 - 4
[51] S. Tricarico, F. Bilotti and L. Vegni, "Multi-functional dipole antennas based on artificial magnetic metamaterials," *Microwaves, Antennas & Propagation*, IET Vol. 4, pp. 1026 – 1038
[52] N. Lopez, L. Cheng-Jung, A. Gummalla and M. Achour, "Compact metamaterial antenna array for long term evolution (LTE) handset application," *iWAT 2009*, pp. 1 – 4
[53] D. Piazza, D. Michele and K. Dandekar, "Two Port Reconfigurable CRLH Leaky Wave Antenna with Improved Impedance Matching and Beam Tuning," EuCAP 2009, pp. 2046 – 2049
[54] D.K.Upadhyay and S. Pal, "Design of Full Scanning Minituarized Antenna Using Left Handed Materials," *in 2011 International Conference on Devices and Communications*, February 2011
[55] V.H. Nguyen, *Advances in Composite Right/Left-Handed Transmission Line Components, Antennas and Systems*, PhD thesis, Ecole Polytechnique de Montreal, January 2010
[56] M. Barati, M. Kaamyab and A.A. Fashi, "Beam Steering Capability Based on Microstrip CRLH Transmission Line," *Progress in Electromagnetics Research Symposium Proceedings*, August 2009, pp. 657 – 661
[57] Y. Nam, L. Liu, Y. Wang, C. Zhang, Joonyoung Cho and Jin-Kyu Han, "Cooperative Communication Technologies for LTE-Advanced," *ICASSP 2010*, pp. 5610 – 5613
[58] C. Caloz, D. R. Jackson and T.Itoh, *Leaky-Wave Antennas*, Publication to appear in unknown**,** October 2010, pp. 29 – 30

[59] Anonymous, *Left-Handed Metamaterial Design Guide*, Ansoft Corporation, Pittsburgh, PA, 2007
[60] D. M. Pozar, *Microwave and RF Design of Wireless Systems*, John Wiley & Sons, November 2000
[61] F.P. Casares-Miranda, E.Marquez-Segura and C. Camacho-Penalosa, "Composite Right/Left-Handed Transmission Line With Wire Bonded Interdigital Capacitor," *LMWC 2006*, Vol. 16, pp. 624 – 626
[62] Anonymous, *Revisions to the DXF Reference*, Chapter 1 DXF Format, [Online] Available: http://www.autodesk.com/techpubs/autocad/acad2000/dxf/dxf_format.htm
[63] Anonymous, *RT/Duroid 5870/5880 High Frequency Laminates*, Rogers Corporation, March 2011, [Online] Available: http://www.rogerscorp.com/acm/products/10/RT-duroid-5870-5880-5880LZ-High-Frequency-Laminates
[64] R.E. Collin, *Foundations for Microwave Engineering*, John Wiley & Sons, 2001
[65] H. Eslambolchi, *LTE TDD versus FDD debate*, [Online] Available: http://www.2020vp.com/hossein-blog/2011/12/lte-tdd-versus-fdd-debate